

MAGNETOSPHERIC ELECTRIC FIELDS MEASURED WITH
DYNAMICS EXPLORER-1

by

Daniel Ray Weimer

A thesis submitted in partial fulfillment
of the requirements for the degree of
Master of Science in Physics
in the Graduate College of
The University of Iowa

May, 1983

Thesis supervisor: Professor Stanley D. Shawhan

Graduate College
The University of Iowa
Iowa City, Iowa

CERTIFICATE OF APPROVAL

MASTER'S THESIS


This is to certify that the Master's thesis of

Daniel Ray Weimer

has been approved by the Examining Committee
for the thesis requirement for the Master of
Science degree in Physics at the May, 1983
graduation.

Thesis committee:


Thesis supervisor


Member


Member

ACKNOWLEDGEMENTS

I wish to thank Stan Shawhan and Don Gurnett for valuable discussions on the DE-1 electric field data and magnetospheric electric fields in general. Credit is due to Richard Huff for his efforts in getting electric field data transferred from NASA/GSFC to the University of Iowa. I thank Terry Averkamp for the utility programs he provided for reading the data tapes and other assistance he gave on using the Physics Department's computer facilities. This research is supported by NASA/GSFC Contracts NAS5-25690 and NAS5-24294.

ABSTRACT

The Plasma Wave Instrument (PWI) on the Dynamics Explorer-1 satellite has been used to measure DC electric fields in the earth's magnetosphere. The DE-1 spacecraft is in an elliptical polar orbit with a radial range of 1.106 to 4.67 R_E . The DC electric field measurements are obtained with two sets of double probes. A long wire antenna with a tip-to-tip length of 215 m measures the electric field in the satellite spin plane. A tubular antenna with a length of 9 m is used for measurements along the spin axis. Data from the sensitive long wire electric field probe is given the most attention. This antenna is rotating with the spacecraft at a rate of one revolution every 6 seconds. By applying a least square error fit to the sinusoidal waveform, the magnitude and orientation of the electric field in the spin plane of the spacecraft is determined. Further computations reduce the measured electric field to components perpendicular and parallel to the magnetic field. Due to the short length of the tubular antenna, the electric field measured along the spin axis shows interference from a non-uniform electric potential around the body of the spacecraft. A simple averaging approach is used to filter some of the interference from the DC measurements. The results of the computations are plotted on graphs with several different formats. One type of graphical output shows the plasma

convection velocity component which is calculated from the electric field measured in the spin plane. These graphs are used extensively in a discussion on polar cap plasma convection. The DE-1 observations affirm the existence of a two-cell circulation pattern. Flow velocities over 2 km/s are seen near the reversals which occur at the center of the convection cells. But the plasma convection pattern is found to be highly variable; the two-cell circulation is often absent. The variations which occur on an orbital and daily basis are compared to changes in the Interplanetary Magnetic Field (IMF) and geomagnetic activity indices. The north-south polarity of the IMF appears to correlate better than the geomagnetic activity with a stronger and more uniform convective flow. Electric field measurements in the auroral zone are discussed. Oppositely directed fields with a magnitude of 100 to 200 mV/m are a common feature, but the absence of "paired electrostatic shocks" of a greater magnitude contradicts measurements with the S3-3 satellite reported in the literature. Electric fields having the paired shock structure which are found in association with field aligned currents have the characteristics of an "auroral vortex." Spectrograms from the Plasma Wave Instrument indicate that these events produce localized plasma waves over a wide frequency range. The final chapter on the observations discusses the relationship between unusual electric fields detected at low latitude concurrent with Stable Auroral Red (SAR) arcs. The electric fields are associated with plasma flows of over 8 Km/s. The phenomenon had been reported before under the name of "Subauroral ion drift", but there had been no previous connection with SAR arcs.

TABLE OF CONTENTS

	Page
LIST OF TABLES	vi
LIST OF FIGURES	vii
CHAPTER	
I. INTRODUCTION	1
II. INSTRUMENTATION	3
III. DATA REDUCTION	6
Data Processing System	6
Calculation of Electric Fields	7
Graphical Display of Data	15
IV. POLAR CAP PLASMA CONVECTION	21
Previous Results	21
DE-1 Results.	23
V. AURORAL ZONE ELECTRIC FIELDS	28
Previous Results.	28
DE-1 Results.	30
VI. STABLE AURORAL RED ARCS.	33
Previous Results.	33
DE-1 Results.	34
VII. DISCUSSION	37
VIII. CONCLUSIONS	39
REFERENCES.	42
APPENDIX A: TABLES	45
APPENDIX B: FIGURES.	47

LIST OF TABLES

Table	Page
1. Characteristics of the Electric Field Sensors in the Plasma Wave Instrument on the Dynamics Explorer-1 Spacecraft	46

LIST OF FIGURES

Figure	Page
1. Graph of electric field strengths measured along the spacecraft Z axis and X axis	48
2. Location of the long wire electric field probes on the DE-1 spacecraft.	50
3. Illustration of the time relationship between successive data records and each measurement.	52
4. Graph of electric field data after computer processing	54
5. Diagram of the orientation of the E_1 electric field at different positions of the DE-1 spacecraft in its orbit.	56
6. Illustration of a case when the magnetic field is not entirely in the spin plane.	58
7. Peak electric field summary plot	60
8. Southern hemisphere plasma convection measured from 6:15 UT to 6:39 UT on day 81343 (December 9, 1981)	62
9. Empirical models of polar cup potentials derived by Heppner to match patterns in the OGO-6 data	64
10. Interplanetary magnetic field data and geomagnetic activity indices for day 81343 (December 9, 1981)	66
11. Southern hemisphere plasma convection measured from 8:06 UT to 8:29 UT on day 81287 (October 14, 1981)	68

Figure	Page
12. Southern hemisphere plasma convection measured from 14:54 UT to 15:17 UT on day 81287 (October 14, 1981)	70
13. Southern hemisphere plasma convection measured from 21:49 UT to 22:14 UT on day 81287 (October 14, 1981)	72
14. Interplanetary magnetic field and geomagnetic activity indices for day 81287 (October 14, 1981)	74
15. Southern hemisphere plasma convection measured from 4:29 UT to 4:53 UT on day 81294 (October 21, 1981)	76
16. Southern hemisphere plasma convection measured from 11:16 UT to 11:39 UT day 81294 (October 21, 1981)	78
17. Southern hemisphere plasma convection measured from 18:08 UT to 18:32 UT day 81294 (October 21, 1981)	80
18. Southern hemisphere plasma convection measured from 1:03 UT to 1:28 UT day 81295 (October 22, 1981)	82
19. Southern hemisphere plasma convection measured from 4:25 UT to 4:50 UT day 81296 (October 23, 1981)	84
20. Southern hemisphere plasma convection measured from 11:12 UT to 11:35 UT day 81296 (October 23, 1981)	86
21. Southern hemisphere plasma convection measured from 4:22 UT to 4:46 UT day 81298 (October 25, 1981)	88
22. Geomagnetic activity indices for the period from day 81294 (October 21, 1981) to day 81298 (October 25, 1981)	90
23. Southern hemisphere plasma convection measured from 8:57 UT to 9:23 UT on day 81364 (December 30, 1981).	92

Figure	Page
24. Interplanetary magnetic field data and geomagnetic activity indices for day 81364 (December 30, 1981)	94
25. Example of oppositely directed electric fields detected on auroral field lines	96
26. Northern hemisphere plasma convection measured from 14:35 UT to 15:35 UT on day 82092 (April 2, 1982)	98
27. High-resolution electric field data for the auroral vortex event at 15:27 UT on day 82092	100
28. Plasma Wave Instrument spectrogram for 14:30 UT to 18:30 UT on day 82092 (April 2, 1982)	102
29. Southern hemisphere plasma convection measured from 22:02 UT to 22:43 UT on day 82108 (April 8, 1982)	104
30. Plasma Wave Instrument spectrogram for 21:30 UT to 23:30 UT on day 82108 (April 18, 1982)	106
31. Example of an unusual, low latitude electric field found on a magnetic field line coincident with an SAR arc	108
32. Electric field measurement from the VEFI experiment on the low-altitude DE-2 spacecraft	110

CHAPTER I

INTRODUCTION

The Dynamics Explorer (DE) spacecraft were launched by the National Aeronautics and Space Administration for the purpose of investigating the coupling between the earth's magnetosphere and ionosphere, and the transfer of energy from the solar wind and solar radiation to the near-earth space environment. The two DE satellites were launched in August of 1981. DE-1 makes measurements primarily in the magnetosphere; the orbit is highly elliptical, with perigee at 675 km ($1.106 R_E$) and apogee at 23,400 km ($4.67 R_E$). DE-2 orbits in the thermosphere at altitudes of 305 to 1300 km. The spacecraft are in coplanar polar orbits. Further details of the Dynamics Explorer program are provided by Hoffman et al. [1981a,b].

The Plasma Wave Instrument (PWI) on DE-1 measures both plasma wave phenomena and quasi-static electric fields. The objective of this paper is to document in detail the techniques used to analyze the data from the electric field measurements, and present initial observations on various electric field phenomena.

Electric fields in the magnetosphere play a key role in the transfer of energy and particles from the solar wind to the magnetosphere, which is defined as a cavity in the streaming solar plasma, inside which the field lines of the planetary magnetic field are

confined. Charged particles in the magnetosphere are transported and accelerated by electric fields. Such fields are thought to be responsible for the aurora or "northern lights," as the phenomenon is more popularly known. A review of the current knowledge of magnetospheric electric fields is given by Stern [1977]. Numerous references are presented in the review.

Although a considerable amount of data has been collected with the Dynamics Explorer spacecraft, limited data processing facilities at NASA have restricted the amount of PWI DC electric field data processed to date. Consequently, this paper will focus on the general nature of the electric field data and on three specific topics:

- (1) The polar cap plasma convection electric field system.
- (2) The auroral zone electric fields and associated plasma wave phenomena.
- (3) The electric fields observed on magnetic field lines coincident with stable auroral red arcs.

CHAPTER II

INSTRUMENTATION

The entire Plasma Wave Instrument on DE-1 is described by Shawhan et al. [1981]. Of concern here are mainly the instrument sub-systems used for D.C. electric field measurements.

Using the double floating probe technique, the electric field is determined from the measurement of the floating potentials of identical probes located in symmetric positions relative to the body of the spacecraft. The difference in the potentials divided by the distance separating the probes gives one vector component of the electric field. Further information about this technique can be found in the papers by Fahleson [1967] and by Cauffman and Gurnett [1972]. The DE-1 spacecraft has two sets of probes. A 9 m tip-to-tip tubular electric antenna is used for electric field measurements along the spin axis of the spacecraft (E_z). A 215 m tip-to-tip long wire antenna perpendicular to the spin axis is used to measure the electric field in the spin plane (E_x) of DE-1.

The tubular electric antenna is constructed from silver-plated BeCu elements, 2.8 cm in diameter and 4 m long. The elements are mounted on opposite ends of the spacecraft directly on the spin axis to eliminate the effects of centrifugal force on the antennas. The spacecraft body is 1 m high, resulting in a total distance of 9 m

between the tips. The inboard 3 m of each element has an insulating coating of teflon. As the plasma potential is measured between the midpoints of the conductors, the effective electrical length is 8 m.

The long wire electric antenna is constructed from BeCu wire with 7 strands, each having a diameter of .005"; five gram masses on each tip serve to hold the wires in an extended position by centrifugal force. The spacecraft spins at a rate of 10 RPM, or one revolution every 6 seconds. The antenna specifications previously published [Shawhan et al., 1981] described the wires as having lengths of 100 m with the inboard 71.1 m insulated with Styland, resulting in an effective DC electrical length of 173.1 m. The construction of the antenna on DE-1 is actually the same as the long antenna on the ISEE-1 spacecraft, which has a tip-to-tip length of 215 m. This is more consistent with an effective electrical length of 186 ± 1 m that is measured.

To minimize the error caused by currents drawn from the space plasma, each antenna is connected to a preamplifier with an input impedance of 10^{10} ohms. The preamplifier outputs are fed to differential amplifiers to obtain the potential difference between antenna elements. There are two differential amplifiers with different gains on both the E_z and E_x antennas. A high-gain amplifier is for measurements of weak electric fields at high resolution, while a low-gain output enables measurements of strong electric fields, which saturate the high-gain amplifier. Table 1 summarizes the measurement range and resolution obtained with each antenna and amplifier. Range switching is not required in the spacecraft electrical system as both output channels on each axis are received on the ground.

The amplifier outputs, which simply are DC voltage levels, are sampled 16 times per second by an analog-to-digital converter with an 8 bit digital output. The raw telemetry data received on the ground for the electric field measurements consists of four sets of integers from 0 to 255 representing measurements spaced apart in time by 62.5 msec. The next chapter describes the procedures required to convert these numbers into scientifically meaningful data.

The Plasma Wave Instrument on DE-1 also has the capability to measure the electric and magnetic components of plasma waves. Certain signatures in the plasma wave spectrograms are correlated with quasi-static electric fields. Examples will be presented in Chapter V. Wave electric fields are measured over a frequency range of 1 Hz to 2 MHz. Wave magnetic fields are sensed with a search coil from 1 Hz to 1 KHz and a loop antenna from 100 Hz to 400 KHz. The step frequency correlator provides a 128-point spectrum from 100 Hz to 400 KHz; the low frequency correlator provides 8-point spectra from 1 Hz to 100 Hz. Spectra are obtained every 32 s for 2 antennas. In addition, high time-resolution data can be obtained through a wideband analog data link. Capabilities of the PWI include distinction between electromagnetic and electrostatic wave phenomena and determination of wave polarization and propagation direction.

The electrical power for the instruments on DE-1 is provided by solar cells. The supply of power is insufficient to operate all of the different instruments continuously. As each instrument has an "on" time of about 50%, there are periodic gaps in the data which are collected.

CHAPTER III

DATA REDUCTION

Data Processing System

The science data which are acquired by the Dynamics Explorer spacecraft are radioed to NASA tracking stations on the ground. All telemetry data are transferred to the Science Data Processing System at Goddard Space Flight Center where it is stored on magnetic tape. The telemetry data must be promoted from the tape data base to on-line computer disk memory for further processing which is done on a Xerox/Honeywell Sigma-9 Computer. Details of the DE Science Data Processing System are described by Smith et al. [1981].

Science investigators located at different sites across the country are responsible for the processing and analysis of the data from the separate instruments on the spacecraft. The DE investigators access the data with remote terminals located at their respective facilities. But the computations required to process all of the data exceeds the capabilities of the relatively small Sigma-9 system. As a result, each of the investigating teams has experienced a slow processing rate. This rate has been marginally adequate for the processing of the Plasma Wave Instrument spectrograms but simultaneous processing of the DC electric field data would have been impractical from the remote terminal. For this reason, the electric field data are

sent on magnetic tape to the University of Iowa where a Univac 418 Computer in the Department of Physics and Astronomy is used for the numerical analysis. A Calcomp microfilm plotter provides for a graphical display of the processed data.

Information about the spacecraft's orbit and attitude is written onto the magnetic tapes along with the "raw" electric field data. This information is vital for the numerical analysis. The process of getting the numbers extracted from the telemetry and orbit/attitude data bases and written onto a tape is initiated from the remote terminal at Iowa. This limits the rate at which data tapes are received. For this reason, the following chapters which describe the scientific results are based on only a small subset of the electric field data which has actually been collected with the Plasma Wave Instrument. Data from about 36 different days has been processed at the present.

Calculation of Electric Fields

The four analog channels, two from E_x and two representing E_z , are multiplexed to a common A/D converter. The converter is designed to have a full-scale digital output of 255 "counts" with an analog input of 5.12 volts. In order to measure both positive and negative electric fields a nominal voltage offset of +2.56 V is added to the outputs of the DC amplifiers. In practice the offset is added to the inputs of the different high/low gain amplifiers, scaled to the gain of the final amplifier stage. With this scheme a digital output of 127 translates to a measurement of 0, while counts of 0 and 255 correspond to respective voltage measurements of -2.54 V and +2.56 V.

A digital output number N is translated to an electric field value with the formula:

$$E = \frac{2.56 (N - N_0)}{G L_{\text{eff}}} \quad (1)$$

N_0 is the integer number representing a value of zero for the electric field. L_{eff} is the effective antenna length and G is the gain of the amplifier. A summary of the relevant parameters for the DC electric field measurements with DE-1 is contained in Table 1. Included in the table are the full scale electric fields and 1 bit resolution of each antenna and amplifier combination. The DC amplifier gains were obtained from instrument calibration measurements on the ground. Table 1 contains two values for the length of the E_x antenna. One is the previously published figure; the other length has been determined from on-orbit "calibration" measurements of the $\underline{V} \times \underline{B}$ electric field, where \underline{V} is the spacecraft velocity. More information about this follows.

The number N_0 used in equation (1) has the nominal value of 127. Examination of the telemetry data, however, revealed that on both axes the simultaneous high-gain and low-gain outputs did not agree. The relative amplitude changes between each step were exactly as expected but there appeared to be a constant DC offset between outputs. On the X axis the high-gain data were at a zero level of 127 while the low-gain output was at 123, which scales to -74 mV/m! Since the antenna is rotating in the electric field the output should follow a sine wave centered on zero. The high-gain numbers had the expected waveform, centered around 127, while the low-gain numbers had a zero

crossing at 123. The obvious method to obtain the proper agreement between channels was to subtract 123 from the low-gain digital values before multiplying by the scale factors to obtain mV/m. With this change in the conversion, the different channels agree to within the 1 bit resolution of the low-gain numbers. A similar offset occurs in the Z axis data, where 124 is subtracted from the low-gain values to obtain the proper agreement. However, since the antenna is not rotating, a sine wave is not available to check the zero-level. The origin of the offset appears to be in the different potentials applied at the inputs of each final amplifier stage in order to bias each output by 2.56 V.

After the conversion of digital counts to mV/m the electric field strengths on the Z axis and X axis can be plotted as a function of time, as in Figure 1. Normally the high-gain data are used due to the higher resolution, but above the saturation levels of the high-gain outputs the low-gain data are selected. The telemetry data from DE-1 are divided into 8 second "records" with 128 data points. Each record has a time-tag in units of milliseconds-of-day (UT). This data format influences the design of these plots and subsequent analysis operations.

The X axis plot in Figure 1 shows the expected sine waveform with a period of 6 seconds. However, the Z axis electric field should be fairly constant, without any spin modulation. The data show "spikes" occurring twice each spin period and a nonsymmetrical spin modulation. This interference on the Z axis has been very persistent during the spacecraft mission, but the magnitude of the noise spikes appears to depend on plasma density. At high altitudes ($2 - 4.5 R_E$) the spikes are

very large and completely mask the true electric field. When the spacecraft enters the plasmasphere the spikes are attenuated, but some spin modulation still exists. The interference seems to be due to differential charging of the spacecraft skin. Similar potential variations--several volts in magnitude--are also detected with the RIMS instrument [R. Chappell, private communication, 1981]. This interference has severely limited the utility of DC electric field measurements with the tubular electric antenna (E_z). Consequently, the data analysis has been concentrated on the measurements with the long wire antenna (E_x). This antenna, in the spacecraft orbit plane, measures the N-S and radial electric fields. As the magnetic field vector generally lies in this plane, electric field components parallel and perpendicular to \underline{B} can be determined. Measurements of the plasma convection component perpendicular to the orbit of the spacecraft can be obtained with the E_x antenna.

From the sine wave measured with the rotating antenna it is necessary to determine the magnitude and direction of the electric field in the spin plane of the DE-1 spacecraft. This determination is carried out with a computer program which does a least square error fit of the data to obtain the magnitude and phase of the sine wave. Each data sample is taken at a specific time; the time difference between the sample time and a reference time is converted to a relative angular position (of the probe antenna) by multiplication of the time difference with the spacecraft's angular rotation rate. The phase obtained with the curve-fitting routine is the angle between the peak of the sine wave and the reference time (angle). The reference is

obtained from the nadir times in the DE data base, derived from earth horizon sensors on DE-1. At the nadir times the +Y axis of the spacecraft is pointing toward the center of the earth. This orientation provides the reference necessary to convert the measured electric field to a known coordinate system, as the vector position of the satellite from the center of the earth is a well known function of time. The Z axis, given in geocentric equatorial inertial (GEI) coordinates, remains relatively constant. The Z axis is perpendicular to the orbit plane. It is maintained to $\pm 1^\circ$. Given the satellite position vector (-Y axis orientation) in GEI coordinates, the X axis is derived from $\underline{Y} \times \underline{Z}$. From the orientations of the X,Y, and Z spacecraft axes, specified as unit vectors in GEI coordinates, one has an orthogonal transformation for converting vectors from GEI coordinates to spacecraft coordinates (and vice versa). This transformation is a function of spacecraft position, hence it changes with time. It must be calculated for each eight second period spanning each record of data. The nadir and positional data are available from the DE orbit-attitude (OA) data base at NASA/GSFC.

The long wire antennas on the DE-1 satellite are mounted at points 15° from the line which defines the Y axis. Since the zero-phase points are assumed to be at the nadir times, it is seen in Figure 2 that there should be a 165° lag between the measured electric field and one directed along the +Y axis. With the magnitude, E_0 , and phase angle, ϕ , of the sine wave determined by the curve fitting routine, the x and y components of the electric field in spacecraft coordinates are obtained from the formulas:

$$E_y = E_o \cos(\phi - 165^\circ) \quad (2a)$$

$$E_x = E_o \sin(\phi - 165^\circ) \quad (2b)$$

The least-squares fit routine works on data spanning one complete, six second spin period. As seen in Figure 1, the electric field may change considerably in one period. Rapid changes in the field can be determined with a greater accuracy by overlapping the time periods in which the curve fitting is done. With the data formatted into eight second records the best way to obtain continuity is to use a two second overlap. This choice results in exactly two measurements or data points for every record (Figure 3). As the data analysis presently is performed by reading data from magnetic tape and writing results to another tape, only two records of input data need to be kept in computer memory at any given time.

Often there may be considerable noise or distortion in the sine wave in regions where there are large and rapid fluctuations in the electric field. Without a "good" sine wave, the magnitude and phase determination may not be accurate. To get some idea of the reliability of the measurements, the error in the curve-fit is calculated. The "chi" coefficient is obtained from the formula:

$$\text{Chi} = \left[\frac{\sum_{i=1}^N \left(\frac{M_i - F_i}{E_o} \right)^2}{N} \right]^{1/2} \quad (3)$$

M_i is the measured electric field at each point i and F_i is the electric field of the sine wave function fitted to the data. The expression for χ in equation (3) is similar, but not identical to the "chi square" calculation normally used in statistical analysis. The error coefficient thus calculated is dimensionless, as the error of each data point is scaled to the sine wave magnitude E_0 . The total number of points, N , is normally 96, unless there are "drop-outs" in the data record. A reasonably good sine wave will have a χ coefficient less than 0.1. If the measured electric field is obscured by noise the curve-fitting algorithm still produces numbers for the magnitude and phase of a sine wave fit. In this case, χ will be greater than one indicating that the fit is not reliable.

The interference on the Z axis can be filtered out to some extent by taking an average (mean) of a number of data points. Since the E_z data are processed simultaneously with the E_x data, considerable simplicity is achieved by averaging over the same six second periods in which the E_x data are analyzed. The standard deviation is calculated for each period as an indicator of the amount of noise present.

A significant proportion of the measured electric field is due to the motion of the satellite through the earth's magnetic field. This $\underline{V} \times \underline{B}$ electric field must be subtracted from the measured electric field to get the true electric field. The vector \underline{V} is the velocity of the spacecraft relative to a frame of reference corotating with the earth. Ideally the spacecraft would measure a three-component electric field vector which could be transformed to GEI coordinates for subtraction of $\underline{V} \times \underline{B}$ and further analysis. But the measurements along

the Z axis and the X-Y plane have different resolution and reliability. Combining the measurements to obtain a vector in GEI coordinates would contaminate the spin plane data with the interference on the Z axis. Therefore most analysis is done entirely in spacecraft coordinates, where the measurements from the different antennas are kept separate. The $\underline{V} \times \underline{B}$ electric field is conveniently calculated in the GEI coordinate system from the numbers in the OA data base at NASA/GSFC. The velocity is calculated from orbital parameters, and \underline{B} is obtained from a model magnetic field rather than magnetometer data. $\underline{V} \times \underline{B}$ is transformed from GEI coordinates to spacecraft coordinates, then subtracted from the measured values of E_x , E_y , and E_z .

When the spacecraft is well within the plasmasphere there should be little electric field other than that from $\underline{V} \times \underline{B}$, provided that the velocity is calculated relative to a plasma which is assumed to be corotating with the earth. This expected result has provided a way to check the calibration of the instrument with the antennas extended while in orbit.

Just after launch the perigee of DE-1 was over the south pole, so that the spacecraft spent very little time in the plasmasphere at L values less than 4 (on magnetic field lines intersecting the equatorial plane at 4 earth radii). These early data had indicated that the phase angle of the electric field measured in the spin plane was off by a constant amount--of the order of 12 to 16 degrees. By early 1982 the perigee had precessed to the equator, so that there was maximum penetration into the plasmasphere. With a large $\underline{V} \times \underline{B}$ electric field it was possible to obtain a more accurate calibration check. An analysis of

two orbits 30 days apart indicated that the phase shift is $16^\circ \pm 1^\circ$, so the computer code which does the data reduction was fine-tuned accordingly. The constant phase shift has been attributed to the capacitor coupling the antennas to the amplifier. In combination with the input impedance of the amplifier this capacitor forms a high-pass filter, which shifts the phase of a signal with a low frequency. The phase shift, as with the constant DC offset in the amplifiers, appears to be stable over time. A phase shift of 10° is expected from the nominal values of the components in the instrument circuit.

The in-orbit calibration was also used to obtain a modified value for the effective length of the spin plane antenna. Originally a length of 173.1 m was assumed. It was found that the magnitude of the electric field was greater than the $\underline{V} \times \underline{B}$ field by a factor of 7%. This factor was the same for both amplifier gains, so the effective antenna length used in the calculation was adjusted to a value of 186 ± 1 m. The electric field measured on the Z axis agreed with expected values, within the limits of the offsets introduced by the spacecraft charging interference.

Graphical Display of Data

After the numerical analysis has been performed, the results must be displayed in a graphical format which can be easily interpreted. It is most economical to perform the time-consuming analysis once, saving the results for use by different plotting routines. The various plotting programs will often access the same data. Interesting features can be replotted with different scale factors to show the finer details without the need for repeating the calculations.

The primary type of display shows the electric fields measured along the Z axis and in the spin plane, with the $\underline{V} \times \underline{B}$ electric field subtracted out. A sample graph is shown in Figure 4. The upper plot is from the six second average of electric fields measured along the Z axis. Immediately below it is a plot of the standard deviation. The next two plots, E_{\perp} and E_{\parallel} , are the components of the spin plane electric field perpendicular and parallel to the magnetic field vector's projection into the spin plane. At the bottom of the graph is the plot for chi, the error coefficient as calculated by equation (3). All data are plotted as a function of time, with the abscissa marked in units of hours and minutes of universal time (UT). Spacecraft position is given in terms of earth radii (R), magnetic latitude (MLAT), magnetic local time (MLT), and McIlwain L-shell parameter (L).

The perpendicular electric field component is calculated from a vector cross product of the measured field with the magnetic field in the spin plane:

$$\frac{E_{\perp} = E_x B_y - E_y B_x}{|\underline{B}|} \quad (4)$$

The resulting number is positive if \underline{E} cross \underline{B} is positive by the "right-hand rule". Since this calculation is done in the spacecraft coordinate system, it is not obvious how E_{\perp} relates to the electric field in the geographic coordinate system. Figure 5 clarifies this matter. In the northern hemisphere a positive E_{\perp} is aligned in the direction of the spacecraft motion. In the southern hemisphere it is just the opposite due to the change in sign of the magnetic field.

The parallel component is obtained simply from the inner product:

$$E_{\parallel} = \frac{E_x B_x + E_y B_y}{|\underline{B}|} \quad (5)$$

One of the objectives of the measurements is to search for parallel electric fields which may be responsible for the acceleration of charged particles in the auroral zones. There are, however, several sources of error which may appear as parallel electric fields which are not real. One cause would be an error in the phase angle adjustment factor which corrects for the instrumental phase shift. An error would cause a truly perpendicular electric field to appear to have a measured parallel component. Likewise, if the electric field has a lot of noise or changes direction rapidly (within 6 seconds) there will be an error in the measured phase angle. In this case χ will be large. Finally, the magnetic field vector may lie at an angle from the spin plane. A convection electric field perpendicular to \underline{B} may have a component in the spin plane that is parallel to the projection of the magnetic field vector. This possibility is illustrated in Figure 6. If \underline{B} lies completely in the spin plane this situation cannot occur. As the geomagnetic pole is tilted from the geographic pole by 11° the angle between \underline{B} and the spin (orbit) plane will vary between 0° and 11° during each day.

There are several instances where fluctuations in the graph of E_{\parallel} match fluctuations in the graph of E_z while the graph of E_{\perp} has a shape of a completely different nature. The ratio of E_{\parallel} to E_z is about 1/5.

The variations in E_{\parallel} due to an East-West (Z axis) electric field component are caused by the offset angle between \underline{B} and the spin plane. But electric field measurements with the long wire antenna usually translate entirely to perpendicular fields. This verifies that the data reduction technique and the associated coordinate transformations are accurate, as magnetohydrodynamic theory predicts that \underline{E} should be perpendicular to \underline{B} .

Electric fields in the auroral zone are expected to have important features which may occur on a size scale much less than the 30 km distance the satellite typically travels in one spin period. The sine wave fit tends to filter out any rapid changes in the electric field which may be important. Likewise, the averaging done on the Z axis data limits both the spatial and time resolution. For this reason a second type of graph which shows peak electric fields is highly useful. An example is shown in Figure 7. The upper plot again shows Z axis data, but with the maximum, minimum, and average fields from each six second period plotted along with the Z component of $\underline{V} \times \underline{B}$. The reduction in the noise spikes in the plasmasphere (after 8:25 UT) is easy to see on this type of graph. The lower plot shows the maximum and minimum fields measured with the long wire antenna, along with the spin plane component of $\underline{V} \times \underline{B}$. Any errors in the calibration factors or the magnetic field data show up clearly on this type of graph. Likewise, the regions where large and rapid fluctuations in E occur, such as the auroral zones, are easy to spot. An example is the peak near 8:19 UT in Figure 7. This peak does not show up in the processed data in Figure 4.

The change in the 1-bit resolution as the data switches from high-gain to low-gain is evident in the peak field plot at 9:02 UT. But even when the peak lies in the low-gain range (low resolution), the electric field strength obtained with the least square error fit has a much better resolution, since the curve-fitting routine works with high-gain data through most of the spin period.

A third type of graph shows plasma convection velocity (East-West), calculated from the electric field in the spin plane (North-South). An example is shown in Figure 8. The position of DE-1 is plotted in magnetic latitude and magnetic local time coordinates on a polar cap projection. The magnetic latitude is obtained from the spacecraft's location through a transformation from the geographic coordinates to a geomagnetic coordinate system. The magnetic local time is obtained directly from the NASA/GSFC OA data base. The plasma convection velocity is drawn as a vector perpendicular to the orbit plane. The vector \underline{U} is calculated from:

$$\underline{U} = (\underline{E} \times \underline{B})/B^2 \quad (6)$$

The lengths of the convection vectors on the graph are proportional to the total magnitude of the vector thus calculated, rather than just the length of a projection of \underline{U} into the equatorial plane. But the directions of the vectors in the figure are obtained by transforming \underline{U} into GEI coordinates. From these coordinates the angle between \underline{U} and the sun vector in the equatorial plane is calculated. The convection vectors are drawn at the same angle with respect to the line connecting

the origin and 12 HRS MLT. The convection plots thus obtained from the DE-1 electric field data in general agree with the well-established pattern of anti-sunward flow over the polar cap and sunward flow at lower latitudes [Stern, 1977]. The plot in Figure 8 is a classic example. But irregular features are often observed in the convection plots; these will be discussed in Chapter IV.

The convection plots generated for the times when DE-1 is above $3 R_E$ do not turn out well for a number of reasons. The spacecraft is moving slower at the high altitude, so successive data points on the plot get blurred together. The magnitude of the magnetic field is very small, so fluctuations in E are magnified through the division by B in equation (6). The electric fields are small, only several mV/m, and rapid fluctuations within one spin period produce a high error coefficient in the data fitting.

CHAPTER IV

POLAR CAP PLASMA CONVECTION

Previous Results

The phenomena of large-scale convection of plasma in the magnetosphere is well-established. The general pattern is that of a two-cell circulation, with anti-sunward flow over the polar cap and sunward flow at lower latitudes. From the interaction of this flow with the magnetic field of the earth, there is a dawn to dusk electric field over the polar cap. In the auroral zones the electric field is oppositely directed, pointing poleward in the evening zone and equatorward in the morning zone.

According to Axford and Hines [1961] the source of the convection is a "viscous-like interaction" between magnetospheric plasma and the solar wind. At the boundary of the magnetosphere the flow is in the direction of the solar wind, and closer to the earth there is a return flow toward the sun. In this view the convective flow is the primary phenomenon and the electric field is the by-product.

An alternative model proposed by Dungey [1961] views the electric field as the primary phenomenon. The field is produced by the flow of the solar wind through "open" magnetic field lines extending from the poles into interplanetary space. The electric field is "mapped" down to low altitudes along the magnetic field lines, which are equipotential

surfaces. Over the poles this field drives the anti-sunward convection; the return flow on closed magnetic field lines is a secondary consequence due to continuity in the plasma flow and electric field.

It is known that there is a high correlation between magnetic activity and the north-south component, B_z , of the interplanetary magnetic field (IMF). This lends support to the model of an open magnetosphere. Likewise, it is expected that the strength of the magnetospheric convection is influenced by the polarity of the IMF [Block, 1973]. A southward IMF should enhance the convection.

The earliest confirmation of the two-lobbed convection pattern by satellite measurement of the electric field was obtained with the Injun 5 spacecraft [Cauffman and Gurnett, 1971]. It is noted that the double-cell pattern represents "a gross simplification of the actual convection, which is often chaotic or turbulent, and variable in time" [Cauffman and Gurnett, 1972]. The Injun 5 data did not reveal a statistically significant relationship between convection magnitude and magnetic activity. It was found that convection magnitudes are often greatest near the reversals, with average velocities of 1.5 km/s. Over the polar region the anti-sunward convection was usually less than 0.75 km/s.

More accurate and continuous measurements were obtained with the OGO 6 probes, but only for a period of about 2 weeks. Contrary to expectations, it was found that the general electric field pattern is not highly variable, even during substorms [Heppner, 1972a]. A correlation was found between substorms and electric fields occurring with a relatively small time and spatial extent, but Heppner pointed out

that there isn't necessarily a direct cause and effect relationship. A dawn-dusk asymmetry in the convection patterns were found to be correlated with the B_y component of the IMF [Heppner, 1972b]. The north-south component of the IMF appears to have been ignored in this paper. From the OGO 6 data empirical models of the polar cap potentials were derived to fit various patterns seen in the electric field [Heppner, 1977]. Examples are shown in Figure 9. Note in Figure 9b the distortion in the two-cell pattern, required to explain multiple reversals seen in the evening auroral zone.

Plasma convection in the ionosphere has also been measured with incoherent scatter radar. These observations have also led to the conclusion that the two-cell convection is not greatly perturbed, but expands equatorward and that velocities are enhanced in response to substorms [Foster et al., 1981].

All of these measurements were obtained at relatively low altitudes. The Injun 5 spacecraft orbited in the range of 680 km to 2530 km altitude, and OGO 6 measured fields from 400 km to 1100 km. As noted earlier, the DE-1 orbit is highly elliptical, with an altitude range of 675 to 23,400 km, so this spacecraft has the opportunity to measure electric fields in unexplored territory.

DE-1 Results

Science operations on the DE-1 spacecraft began in October of 1981, after a month-long sequence of attitude adjustment and instrument activation. At this time orbit apogee was over the north pole and perigee was over the south pole. This enabled the observation of con-

vection in the southern hemisphere during the initial months of operation.

The limited amount of data processed so far have indicated that the convection can be highly irregular in structure. Only on rare occasions is an undisturbed two-cell pattern seen. Significant changes occur from day to day, and even from one orbit to the next (the orbital period is about 7 hours). At the times for which interplanetary magnetic field data are available the evidence supports the view that a southward IMF produces a strong convective flow. Correlation with indices of geomagnetic activity is weaker. Dips in the hourly equatorial D_{st} index appear to correlate better than the three hour K_p index. Enhanced polar convection seen at times of high geomagnetic activity may be a coincidence due to the fact that substorms usually occur when the Z component of the IMF is negative.

Figure 8 shows a convection plot from day 81343. (This notation refers to the 343rd day, December 9, of the year 1981.) Plots of B_z , D_{st} , and K_p for day 81343 are in Figure 10. Preceding the time of the measurement in Figure 8, B_z was negative and D_{st} had dropped slightly, which is indicative of an increase in the extraterrestrial ring current. At the time of the measurement, B_z turned positive. It is reasonable to expect a time delay between changes in the IMF, as measured with spacecraft orbiting beyond the bow shock, and the effects seen in the near-earth magnetosphere.

The variability in the convection is illustrated in the graphs from three consecutive orbits shown in Figures 11 to 13. Figure 14 contains the geomagnetic indices and IMF data for this period. The anti-sunward

flow over the polar cap is irregular in Figures 11 and 12. During this time from 5 to 15 hours UT on day 81287 both the K_p and D_{st} indices were recovering from levels indicative of a high disturbance in the geomagnetic field. From 16 to 24 hours UT K_p steadily increased from 3+ to 6- coincident with a southward turning of the IMF. At 22:00 UT the convection flow in Figure 13 is seen to be enhanced.

Another sequence of plots spanning the period from day 81294 (Oct. 21, 1981) to day 81298 (Oct. 25, 1981) is presented in Figures 15 through 21. There is no IMF data available for this period, but some correlations can be made with the magnetic activity, given in Figure 22. At the time when the data in Figure 15 were obtained, the magnetic activity is high. The convection is fairly uniform with the exception of the reversal at $65^\circ - 72^\circ$ MLAT in the evening sector. This type of pattern agrees with Heppner's model in Figure 9b. In Figure 16 there is no large-scale pattern in the convective flow. There are localized regions where a strong flow occurs in one direction then reverses. These are most likely associated with field-aligned currents as described in the next chapter. Figure 17 indicates almost no convection; K_p reached a low of 2+ during this time. One orbit later, in Figure 18, the familiar pattern is seen. The D_{st} index had dipped slightly and K_p was on the rise. On the next day the flow is weak and the region of anti-sunward flow has expanded, as shown in Figure 19. One orbit later (Figure 20) the convection has become erratic. The features at 50° to 75° MLAT in the evening sector in Figure 19 appear to have "evolved" to the pattern seen in Figure 20. Figure 21 again shows a two-cell convective flow at the same time that the D_{st}

index takes a dip. The largest convection magnitude is seen just equatorward of the reversals. A component over 2 km/s occurs at one point. This agrees with the trend seen in the Injun 5 data [Cauffman and Gurnett, 1972].

The best plasma flow pattern seen in the data processed to date is shown in Figure 23. These data were obtained on day 81364 (Dec. 30, 1981). The geomagnetic and IMF data for this day are displayed in Figure 24. Preceding the pass of DE-1 over the pole, the D_{st} index had dropped to -80 gammas coincident with a southward turn in the interplanetary magnetic field. The K_p index at this time was 4-indicating moderate magnetic activity. Since there are several cases where K_p is much higher while the convective flow is weaker, there does not appear to be a direct link between the two.

There is a relationship between features on the convection graphs and patterns in the plasma wave spectrograms obtained with the Plasma Wave Instrument. The regions of sunward flow usually have intense, right-hand polarized, whistler-mode radiation at frequencies of 300 Hz to 20 kHz. The region of anti-sunward flow is very quiet. In contrast, at the point where the reversal occurs there is often a noise burst at all frequencies from 1 Hz up to 400 kHz. Although the noise spans the frequency range, the wave energy peaks below 60 Hz. This is consistent with "velocity shear driven plasma turbulence" detected with the Hawkeye 1 spacecraft [Kintner, 1976]. The turbulence is indicated by both electric and magnetic fluctuations which do not propagate from the source. The high frequency components, however, do not agree with Kintner's observations. Phase measurements with the DE-1 PWI indicate

that the components above 100 Hz are sometimes well correlated, with a right-polarized mode. To add to the confusion, the noise bursts are often found well within the region of sunward plasma flow at the points where the electric field reaches a peak. Examples are presented in Chapter V.

CHAPTER V

AURORAL ZONE ELECTRIC FIELDS

Previous Results

The precise nature of the relationship between the aurora and magnetospheric electric fields has yet to be determined. From the Injun 5 data it was established that the electric field reversals occur in the auroral zone, at invariant latitudes of 60° to 80° [Cauffman and Gurnett, 1972]. The reversal is considered to occur at the boundary between open and closed magnetic field lines. It was noted by Frank and Gurnett [1971] that this boundary is coincident with the energetic electron ($E > 45$ kev) trapping boundary. Furthermore, the reversals were found to be associated with "inverted V" electron precipitation events, so called because of a characteristic shape in graphs of electron energy vs. time. The electron precipitation involves a considerable field-aligned "Birkeland" current. In the neighborhood of the "inverted V" events the electric field had large (125 mV/m) and irregular fluctuations, often consisting of distinct pairs of oppositely directed spikes [Gurnett, 1972].

With the S3-3 satellite, Mozer et al. [1977] have observed oppositely directed, perpendicular electric fields of a similar nature but with a much larger magnitude (>400 mV/m). Large parallel electric field components over 400 mV/m were found between the "paired electrostatic shocks". Other instruments on S3-3 identified magnetic

field-aligned currents and extreme plasma turbulence in the regions of the shocks. Mozer identified the wave turbulence as electrostatic ion cyclotron waves.

The S3-3 satellite had provided measurements at altitudes from about 260 km to the satellite apogee at 8000 km. A quasi-static electric field experiment on the ISEE-1 satellite has measured electrostatic shock "events" at geocentric distances between 2.9 and 6.5 R_E [Mozer, 1980]. In this paper, "an 'event' was defined as an interval of > 10 Hz electric field turbulence within which the quasi-static electric field magnitude somewhere exceeded about 100 mV/m". Mozer argues that "the duration and field strengths of these events suggest that the auroral particle acceleration region is confined to altitudes less than a few R_E and that the highest altitude observations are due to mapping of electric fields from the acceleration region to the point of observation" [1980].

A different view of a qualitatively similar phenomenon is given by Burk, Silevitch, and Hardy [1982]. Their analysis is based on data from the S3-2 satellite flying at altitudes of 240 km to 1557 km. They characterize the events as "small-scale auroral vortices", marked by large deflections in the east-west magnetic field component measured on the spacecraft, indicative of downward and upward current sheets, which are also observed in the particle spectra. In the region between current sheets the electric field rotated by 180° then returned to the original orientation. The magnitude of the fields can exceed 200 mV/m. The plasma flow is viewed as having "two vortices with clockwise and

counterclockwise rotations around the positively and negatively charged flux tubes, respectively".

DE-1 Results

The DE-1 measurements of auroral zone electric fields both reaffirm some of the previous observations and introduce some new questions. Electric fields with the general character of an "electrostatic shock" are seen, but none have ever been observed with the large magnitudes reported by Mozer. The electric fields detected with the DE-1 long wire antenna never exceed 200 mV/m in the cases processed to date.

One case of a shock-like event is shown in Figure 25. These data are from a time when DE-1 was in the northern hemisphere at an invariant latitude of 65.3° and altitude of 9,000 km (2.42 Re). At 3:45:02 UT (28 seconds from start of plot), there is an electric field of 90 mV/m. After the antenna rotates 180° there is a field with the same sign at a magnitude of 160 mV/m. This field is pointing in the opposite direction from the one encountered 3 seconds earlier. The separation is 16 km as the satellite was moving 5.46 km/s. At this time DE-1 was directly on a magnetic field line connected with a source of auroral hiss. This is determined from the plasma wave frequency-time spectrogram which shows a "funnel-shaped" feature centered on the event. This type of spectral feature is explained by Gurnett et al. [1983]. The funnel shape is "a propagation effect caused by a frequency dependence beaming of the whistler mode radiation along the magnetic field." It is indicative that the source of the auroral hiss was located a distance below the spacecraft.

At lower altitudes events consistent with the "auroral vortex" theory are often seen. As mentioned before, the plasma convection velocity often has the largest magnitude near the reversals, usually in the sunward flowing regions. The PWI spectrograms show broadband noise at these events. The electric field looks as if a perturbation had been added to the uniform convection field. The perturbation field consists of oppositely directed fields. The data from the magnetometer on DE-1 indicate that these fields are associated with field-aligned currents. A similar correlation between the electric and magnetic fields is seen on the DE-2 satellite [Sugiura et al., 1982].

The best examples of vortices are found near the cusp. One case is shown in Figure 26. The peak near 64° MLAT on the convection graph occurred at 15:27:40 UT on day 82092. Figure 27 shows high-resolution data where the electric field measured in the spin-plane reaches a peak then reverses. The field along the spacecraft Z axis also shows a large variation at this point, of the order of 350 mV/m. As the magnetic field is co-planar with the spin-plane and perpendicular to the Z axis, this indicates that the electric field is rotating around in a plane perpendicular to \underline{B} . Summary data from the DE-1 magnetometer shows a perturbation of 500 nT in the east-west magnetic field due to field-aligned currents. Figure 28 contains the plasma wave spectrogram for this time. The broadband noise burst is clearly visible. This plot also shows the relatively quiet region where the plasma flow is antisunward before 15:25 UT, and the occurrence of whistler-mode radiation in the sunward flowing plasma after 15:25 UT.

A very interesting case was found in the southern hemisphere 16 days later. (By this time in 1982 the orbit had precessed such that perigee was near the equator and both poles were crossed at roughly equal altitudes.) Figures 29 and 30 show a convection plot and spectrogram containing two events of interest. The noise burst at 22:09 UT corresponds to the peak in the morning sector. There is a pair of opposing electric fields in the evening sector at 22:24 UT corresponding to another broadband line in the spectrogram. The DC electric field reaches 140 mV/m in this event.

The plasma waves have both electric and magnetic components. The narrow vertical shapes on the frequency-time spectrograms indicate that the disturbances are highly localized on specific field lines. In the event of 22:09 UT on day 82108 (Figure 30), the DE-1 spacecraft, at a distance of $1.5 R_E$, must have been very close to the source region. The same is true of the case shown in Figure 28, but some spread is seen in the spectrogram above 10 KHz. There is a greater spread at the second event in Figure 30. These are of the same nature as the "funnel shapes" encountered when DE-1 is at distances above $2 R_E$ [Gurnett et al., 1983] but the components above 100 KHz were never seen at the greater distances. The components above 100 Hz are usually correlated, with a right-polarized mode.

The mechanism by which the noise bursts are generated has yet to be determined. One possibility is the current driven ion cyclotron instability associated with non-uniform magnetic shear. More work needs to be done to see if the observations are consistent with a theory described by Bakshi et al. [1983].

CHAPTER VI

STABLE AURORAL RED ARCS

Previous Results

Stable auroral red (SAR) arcs generally occur at mid-latitudes during geomagnetic storms. These arcs are unusual in that they occur well equatorward of the auroral zone and their intensity does not vary greatly with time. The light from these arcs is from the red 630 nm emission line of atomic oxygen, at subvisual intensities. The emission occurs at an altitude of about 400 km. A review of the characteristics of SAR arcs is given by Rees and Roble [1975]. It is known that the arcs occur on magnetic field lines connected with the plasmopause region. Satellite measurements have found that in the region of SAR arc emission there is a depression in the electron density and an enhancement in the electron temperature. Collisions between atomic oxygen and electrons with energy greater than 2 eV excite the atoms which produce the 630 nm radiation.

It has been proposed that perpendicular electric fields could produce an SAR arc by providing the energy to heat the electrons. Rees and Roble [1975] discount this hypothesis on the basis of their own theoretical calculations. Additionally, electric fields had previously never been observed in SAR arcs.

DE-1 Results

The DE-1 data had indicated the occasional presence of stable, large-scale electric fields at low invariant latitudes. On the basis of information provided by Nagy and Kozyra [private communication, 1982] it has been found that these unusual fields are found on magnetic field lines coincident with reported SAR arcs. Several cases have been found. The electric fields have a very distinct character. An example is given in Figure 31, from day 81293. After the pass through the auroral zone, where the electric field is fairly noisy, a very smooth perpendicular field is encountered at 14:09 UT. The field reaches a peak of 27 mV/m after 14:11 UT, then drops off abruptly. An SAR arc was detected by ground-based photometers on the same day at the same invariant latitude (53°) where the electric field reaches the peak. The plasma convection associated with the peak field is about 8 km/s, directed westward, opposite to corotation. This occurs on an L shell which is normally considered to be well within the corotating plasmasphere. The long "tail" on the electric field plot extending to 14:20 UT is indicative that the plasmasphere is "slipping". It is an artifact of the $\underline{V} \times \underline{B}$ calculation in which the spacecraft velocity is relative to a corotating frame of reference. The plasma observed by the spacecraft from 14:12 UT to 14:20 UT is gradually speeding up to match corotation as the spacecraft moves in to lower L values. This particular event is associated with a magnetic substorm which started 6 hours prior to the observation, at which time the K_p index was 7-.

The Vector Electric Field Instrument (VEFI) on the low-altitude DE-2 spacecraft measured a similar electric field on nearly coincident

magnetic field lines. This instrument is described by Maynard et al. [1981]. The magnitude measured with VEFI was much higher due to magnetic field line convergence at lower altitudes. Data provided by N. Maynard of NASA/GSFC is shown in Figure 32. DE-2 was in the southern hemisphere moving toward a higher invariant latitude as time increases, so the electric field is almost a mirror image of the graph in Figure 31. The ratio of the electric field magnitudes measured with DE-1 and DE-2 is found to be in agreement with the equation:

$$\frac{E_1}{E_2} = \left(\frac{R_2}{R_1} \right)^{3/2} \quad (7)$$

This is an approximate equation for the electric fields found at different radial distances on the same magnetic field line. This equation is based on the assumption that the field lines are equipotentials.

According to Maynard the langmuir probe on DE-2 had measured an increase in the electron temperature and a decrease in the electron density coincident with the peak in the electric field measured with VEFI [DE Science Team meeting, Feb. 1983]. This is consistent with the characteristics of SAR arcs mentioned before [Rees and Roble, 1975]. The DE-1 PWI spectrograms usually show the presence of intensified VLF plasmaspheric hiss where the large electric fields are encountered, indicative of an elevated electron temperature.

The type of electric field and plasma convection described here has been observed with other spacecraft. Spiro et al. [1979] refer to the phenomena as sub-auroral ion drift (SAID) in a report on AE-C ion drift measurements. Maynard et al. (1980) saw a case in the ISEE-1 electric field data. The SAID events occur predominately in the local time sector between 18:00 hrs and 2:00 hrs. Their occurrence is associated with magnetic substorms, but no previous connection has been made with SAR arcs. The SAID events are in agreement with a modeling of substorms by Harel et al. [1980a,b] and Spiro et al. [1980].

Even though large electric fields are found coincident with SAR arcs, it is not conclusive that the fields are directly responsible for producing the arcs. There are times when no electric fields were seen when DE-1 was on magnetic field lines on which SAR arcs were observed on the ground. One such case is the SAR arc event described by Kozyra et al. [1982]. The SAR arcs also have a nearly global longitudinal extent, whereas the SAID events are confined to locations around 21:00 hrs local time. The relationship between the SAR arcs and SAID is most likely that both occur on the edge of the plasmaphere when it moves inward during magnetic substorms.

CHAPTER VII

DISCUSSION

The analysis of the DC electric field data from DE-1 is obviously not a trivial task. Considerable time was spent over a nine month period in developing the computer programs which convert the data from digital bits to graphic displays. Every step of the development had to be checked carefully to insure that the intermediate results were consistent with the input data. Several plotting programs are required to display the data in different formats, such as peak electric fields or calculated convection velocity component. In addition utility programs were required for such tasks as listing on a printer the data and orbital information for specific time periods. Program efficiency was also a consideration, since it takes one hour of computer time to process 12 hours of real-time data. Once the main analysis program was known to be functioning correctly it was completely restructured in order to obtain a 3:1 increase in efficiency. (This included the elimination of a time-consuming printout of every computed value, required in the early stages for diagnostic purposes.)

The results obtained so far are consistent with previous electric field measurements. But the data have always yielded new information due to the excellent sensitivity of the long wire antenna and the unique orbit of the spacecraft.

The convection graphs are very useful in understanding various magnetospheric processes, such as the merging of the earth's magnetic field with the interplanetary field carried by the solar wind. But due to the complexity of the situation a statistically significant number of cases must be collected before definite conclusions can be reached.

Numerous auroral passes have been collected in the data base. Since the mechanism by which the aurora are produced is not completely understood there is opportunity for making new discoveries. Information about the electric fields is of vital importance, but simultaneous data from other instruments is required. A comprehensive analysis is beyond the intent of this paper, but observations reported in Chapter V could form the basis of such an investigation. Of particular interest are the plasma waves found coincident with the oppositely directed DC electric fields on auroral field lines.

The subauroral ion drift phenomenon had been detected before, but previously there had been no connection with SAR arcs. A direct cause and effect relationship may not even exist. This subject is currently under investigation in collaboration with scientists at the University of Michigan Space Physics Research Laboratory. The identical patterns seen in both the DE-1 and DE-2 electric field data at a magnetic conjunction verify that the analysis techniques are correct.

CHAPTER VIII

CONCLUSIONS

The short tubular electric antenna on DE-1 has been of limited use for DC electric field measurements due to the interference which masks the true field values. In the plasmasphere, where the plasma density is higher, the interference is highly attenuated and the measured field matches the calculated $\underline{V} \times \underline{B}$ field fairly well. On occasion, there will be changes detected with the short antenna which match features in the spin plane data. The measurement along the spin axis then gives an indication of the three dimensional structure of the electric field.

In contrast, the long wire antenna has provided excellent data on the electric field in the spacecraft spin plane. The magnitude of the field can be determined to within 0.42 mV/m. The spatial and time resolution is limited by the 6 second rotational period. For most of the electric field phenomenon observed, this hasn't been highly detrimental.

Measurements of the polar cap plasma convection patterns have been very illuminating. Significant changes occur from one day to the next, and even on successive spacecraft orbits there are large variations. This indicates that the convective flow is not a constant steady-state but is influenced greatly by outside forces. There is not a direct

correlation between geomagnetic activity and the strength or uniformity of the polar cap plasma convection. The most important factor appears to be the polarity of the north-south component of the interplanetary magnetic field. A southward IMF produces a distinct two-cell convection pattern. This supports the theory of an "open" magnetosphere with the field lines in the polar regions merging with the interplanetary field. The electric field in the solar wind is connected to the ionospheric plasma along the open field lines.

At times a two-cell convective flow is not seen. Then the passes over the polar cap are characterized by localized regions of rapid flow. Even when the two-cell pattern is seen, there are enhancements to the electric field near the boundary between sunward plasma flow and antisunward flow. The peaks in the electric field often occur in pairs pointing in opposite directions. Magnetometer data indicate that these events are associated with field aligned currents which produce a vortex in the plasma flow. When only one peak is seen in the electric field, it may be because the path of the spacecraft through the region did not intercept both peaks. Coincident with the field aligned current events, the plasma wave instrument detects the presence of intense plasma wave oscillations. The disturbances have both electric and magnetic components, sometimes with a definite right circular polarization. It occurs at a wide range of frequencies from 1 Hz up to over 300 kHz. The source region of the plasma oscillations is found at a radial distance of $1.5 R_E$.

The oppositely directed electric fields seen in the DE-1 data are consistent in character with similar events previously reported in the

literature. The field reversals occur on a region 10 to 30 km across. But the magnitudes measured with DE-1 are not as large as previously reported by Mozer et al. [1977]. This could be due to a difference in the response of the instruments to rapid changes in the DC field. But it is possible that as more DE-1 data is processed electric fields will be found with magnitudes greater than 200 mV/m.

A correlation has been found between unusual low-latitude electric fields and SAR arcs. The electric field corresponds to a plasma flow directed opposite to corotation. As this phenomenon had previously been discovered with ion drift detectors it had been given the name "subauroral ion drift". The boundary region between the corotating plasma and the SAID contains plasma which is virtually standing still in the inertial (GEI) reference frame. The peak in the electric field or plasma flow is found to be on SAR arc field lines. The exact mechanism by which the SAR arcs are produced is yet to be determined. The electric field could be responsible for heating the electrons which produce the arcs. Electrons accelerated by the electric field would be heated by collisions in the ionosphere. But the fact that the arcs can occur without the electric field adds to the mystery.

REFERENCES

- Axford, W. I., and C. D. Hines, A unifying theory of high-latitude geophysical phenomena and geomagnetic storms, Can. J. Phys., 39, 1433, 1961.
- Bakshi, P., and G. Ganguli, and Palmadesso, Finite width currents, non-uniform magnetic shear and the current driver ion cyclotron instability, NRL Memorandum Report 5034, 1983.
- Block, L. P., The Magnetosphere, Ch. 8, Cosmical Geophysics, Scandinavian University Books, 1973.
- Burke, W. J., M. Silevitch, and D. A. Hardy, Observations of small-scale auroral vortices by the S3-2 satellite, 1982 preprint.
- Cauffman, D. P., and D. A. Gurnett, Double-probe measurements of convection electric fields with the Injun-5 satellite, J. Geophys. Res., 76, 6014-6027, 1971.
- Cauffman, D. P., and D. A. Gurnett, Satellite measurements of high latitude convection electric fields, Space Science Reviews, 13, 369-410, 1972.
- Dungey, J. W., Interplanetary magnetic field and the auroral zones, Phys. Rev. Lett., 6, 47-48, 1961.
- Fahleson, U., Theory of electric field measurements conducted in the magnetosphere with electric probes, Space Science Reviews, 7, 238-262, 1967.
- Foster, J. C., J. R. Duvnito, and G. S. Stiles, Large scale patterns of auroral ionospheric convection observed with the chatanika radar, J. Geophys. Res., 86, 11, 357, 1981.
- Frank, L. A., and D. A. Gurnett, Distributions of plasmas and electric fields over the auroral zones and polar caps, J. Geophys. Res., 76, 6829, 1971.
- Gurnett, D. A., Electric field and plasma observations in the magnetosphere, proceedings of the symposium jointly sponsored by COSPAR, IAGA, and URSI, 11-13 May 1972, p. 123-138.

- Gurnett, D. A., S. D. Shawhan, and R. R. Shaw, Auroral hiss z-mode radiation and auroral kilometric radiation in the polar magnetosphere: DE-1 observations, J. Geophys. Res., 88, 329-340, 1983.
- Harel, M., R. A. Wolf, P. H. Reiffe, R. W. Spiro, W. J. Burke, F. J. Rich, and M. Smiddy, Quantitative simulation of a magnetospheric substorm, 1. model logic and overview, J. Geophys. Res., 86, 2217, 1981.
- Heppner, J. P., Electric field variations during substorms: Ogo-6 measurements, Planet Space Sci., 20, 1475, 1972a.
- Heppner, J. P., Polar-cap electric field distributions related to the interplanetary magnetic field direction, J. Geophys. Res., 77, 4877, 1972b.
- Heppner, J. P., Empirical models of high-latitude electric fields, J. Geophys. Res., 82, 1115, 1977.
- Hoffman, R. A., and E. R. Schmerling, Dynamics Explorer program: an overview, Space Sci. Instr., 5, 345, 1981a.
- Hoffman, R. A., G. D. Hogan, and R. C. Maehl, Dynamics Explorer spacecraft and ground operations systems, Space Sci. Instr., 5, 349, 1981b.
- Kintner, P. M., Observations of velocity shear driven plasma turbulence, J. Geophys. Res., 81, 5114, 1976.
- Kozyra, J. U., T. E. Cravens, A. F. Nagy, M. O. Chandler, L. H. Brace, N. C. Maynard, D. W. Slater, B. A. Emery, and S. D. Shawhan, Characteristics of a stable auroral red arc event, Geophys. Res. Lett., 9, 973-976, 1982.
- Maynard, N. C., T. L. Aggson, and J. P. Heppner, Magnetospheric observations of large subauroral electric fields, Geophys. Res. Lett., 7, 881, 1980.
- Maynard, N. C., E. A. Bielecki, and H. F. Burdick, Instrumentation for vector electric field measurements from DE-B, Space Science Instr., 5, 523-534, 1981.
- Mozer, F. S., ISEE-1 observations of electrostatic shocks on auroral zone field lines between 2.5 and 7 earth radii, University of California preprint, 1980.
- Mozer, F. S., C. W. Carlson, M. K. Hudson, R. B. Torbert, B. Parady, and J. Yatteau, Observations of paired electrostatic shocks in the polar magnetosphere, Phys. Rev. Lett., 38, 292, 1977.

- Rees, M. H. and R. G. Roble, Observations and theory of the formation of stable auroral red arcs, Rev. Geophys. and Space Physics, 13, 201, 1975.
- Shawhan, S. D., and D. A. Gurnett, D. A. Odem, R. A. Helliwell, and Chung G. Park, The plasma wave instrument and quasi-state electric field instrument (PWI) for Dynamics Explorer-A., Space Sci. Instru., 5, 535, 1981.
- Smith, P. H., C. H. Freeman, and R. A. Hoffman, Dynamic Explorer science data processing system, Space Science Instru., 5, 561-573, 1981.
- Spiro, R. W., R. A. Heelio, and W. B. Hanson, Rapid subauroral ion drifts observed by Atmosphere Explorer C, Geophys. Res. Lett., 6, 657, 1979.
- Spiro, R. W., and M. Harel, R. A. Wolf, and P. H. Reiff, Quantitative simulation of a magnetospheric substorm, 3. Plasmaspheric electric fields and evolution of the plasmopause, J. Geophys. Res., 86, 2261, 1981.
- Stern, D. P., Large-scale electric fields in the earth's magnetosphere, Rev. Geophys. and Space Phys., 15, 156, 1977.
- Sugiura, M., N. C. Maynard, W. H. Farthing, J. P. Heppner, B. G. Ledley, and L. J. Cahill, Initial results on the correlation between the magnetic and electric fields observed from the DE-2 satellite in the field-aligned current regions, Geophys. Res. Lett., 9, 985, 1982.

APPENDIX A:

TABLES

TABLE 1

Characteristics of the Electric Field Sensors in the Plasma Wave
Instrument on the Dynamics Explorer-1 Spacecraft

	Effective DC Antenna Length	Amplifier Gain	Full Scale Electric Field	Digital Resolution
E_z Low Gain	8 m	0.178	1.8 V/m	14 mV/m
E_z High Gain		1.78	180 mV/m	1.4 mV/m
E_x Low Gain				
Design	173.1 m	0.0062	2.38 V/m	19 mV/m
Calibrated	186 m		2.22 V/m	17.3 mV/m
E_x High Gain				
Design	173.1 m	0.254	58 mV/m	0.45 mV/m
Calibrated	186 m		54 mV/m	0.42 mV/m

APPENDIX B

FIGURES

Figure 1

Graph of electric field strengths measured along the spacecraft Z axis and X axis. The data shown spans a 72 second period. On this time scale, the sine wave modulation on the X axis is clearly visible. The modulation is due to the rotation of the spacecraft once every six seconds. The Z axis data also shows a spin modulation which should not be present, as the probes are parallel to the spin axis.

A-683-294

UNIVERSITY OF IOWA
DE-1 PLASMA WAVE INSTRUMENT DC ELECTRIC FIELD
ORBIT 281 DAY 81295 UT 14: 8:12 - 14: 9:24

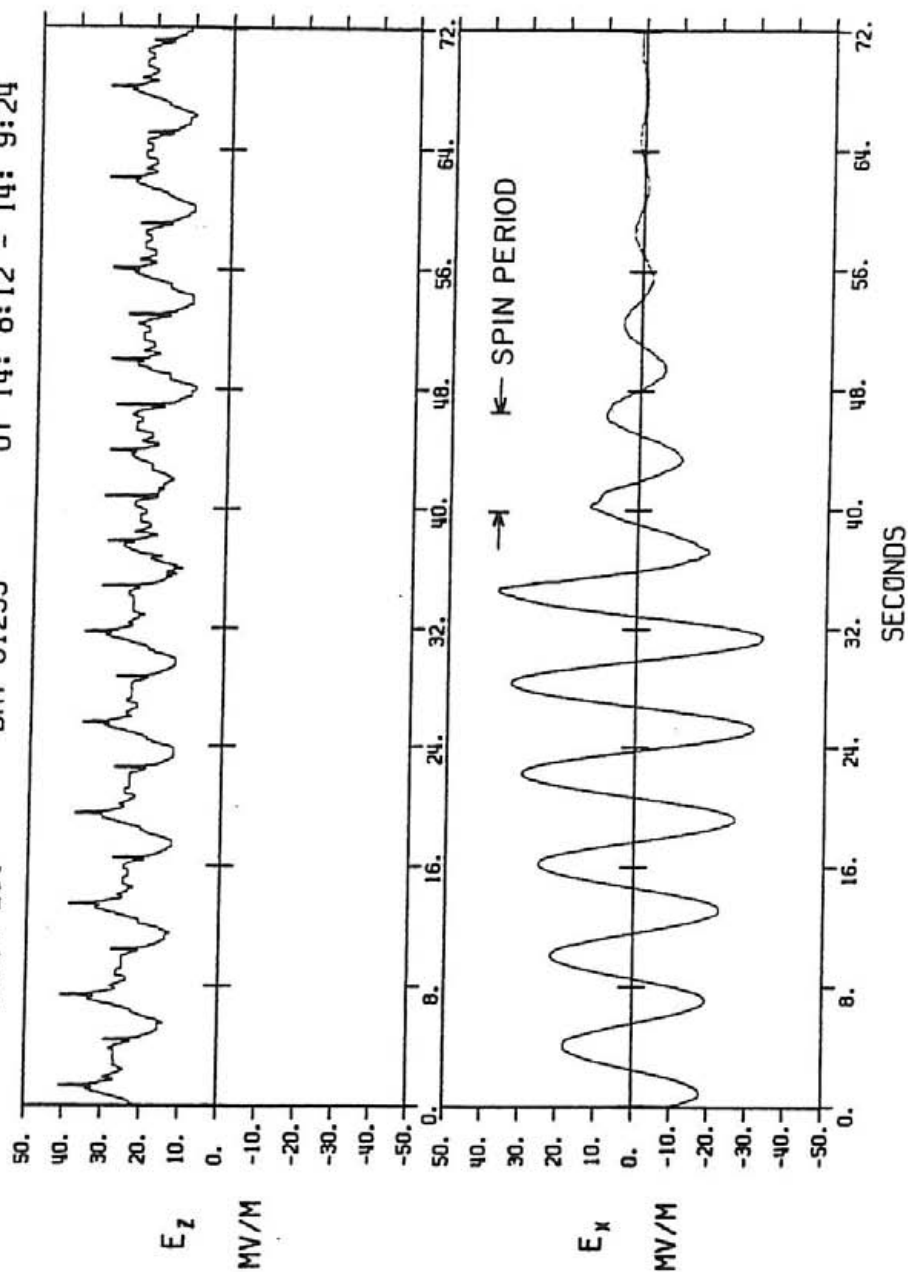


Figure 1

Figure 2

Location of the long wire electric field probes on the DE-1 spacecraft. Due to the 15° offset between the probes and the Y axis, there should be a 165° lag between the time at which the +Y axis is pointing to earth center and the time at which the electric field is being measured in the same direction.

A-G83-171

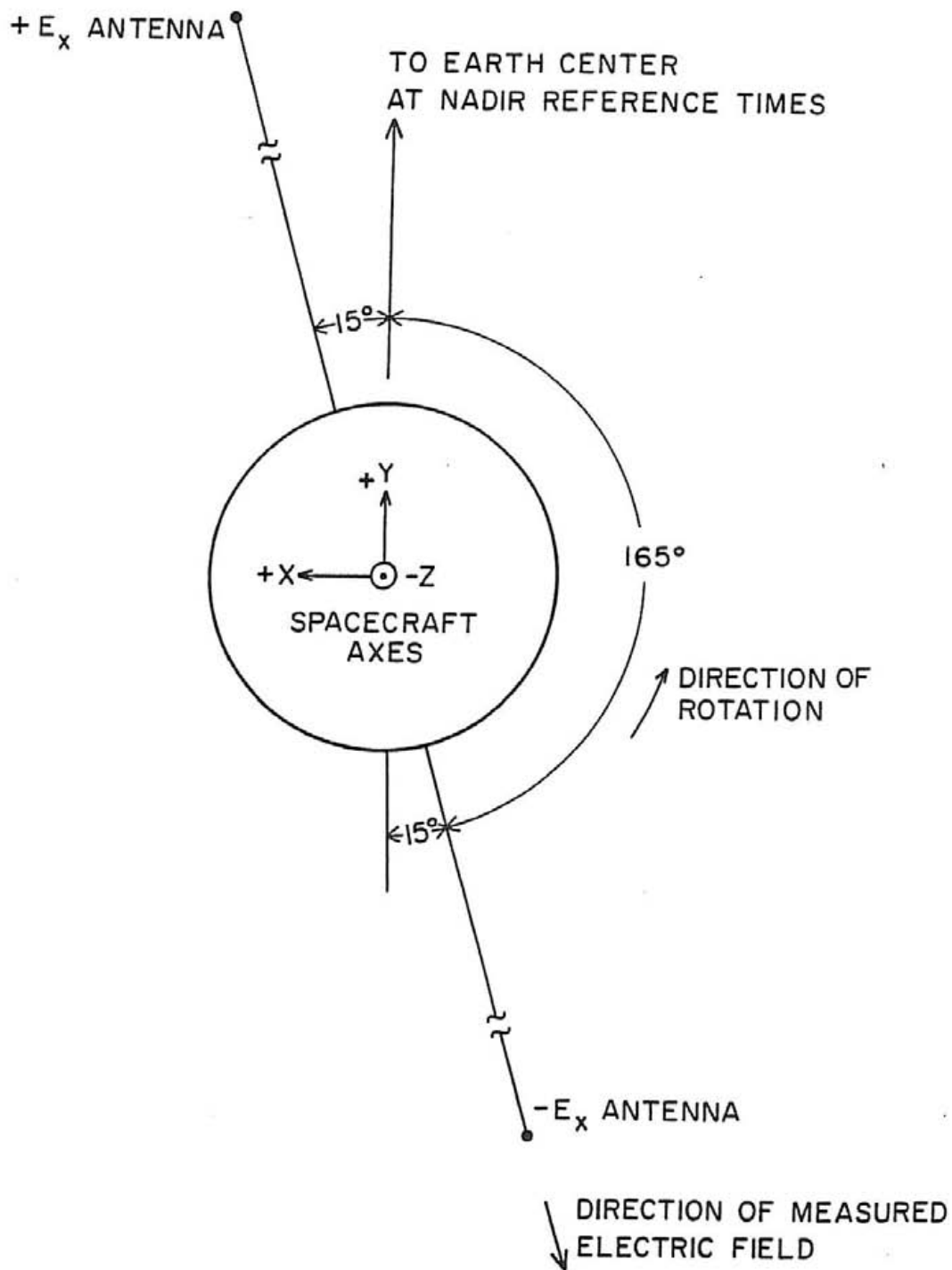


Figure 2

Figure 3

Illustration of the time relationship between successive data records and each measurement. The data is grouped into records spanning 8 seconds of time. The analysis is performed on segments of data spanning 6 seconds of time, with a 2 second overlap between adjacent segments. This results in measurements spaced 4 seconds apart, or two per data record.

A - G83 - 172

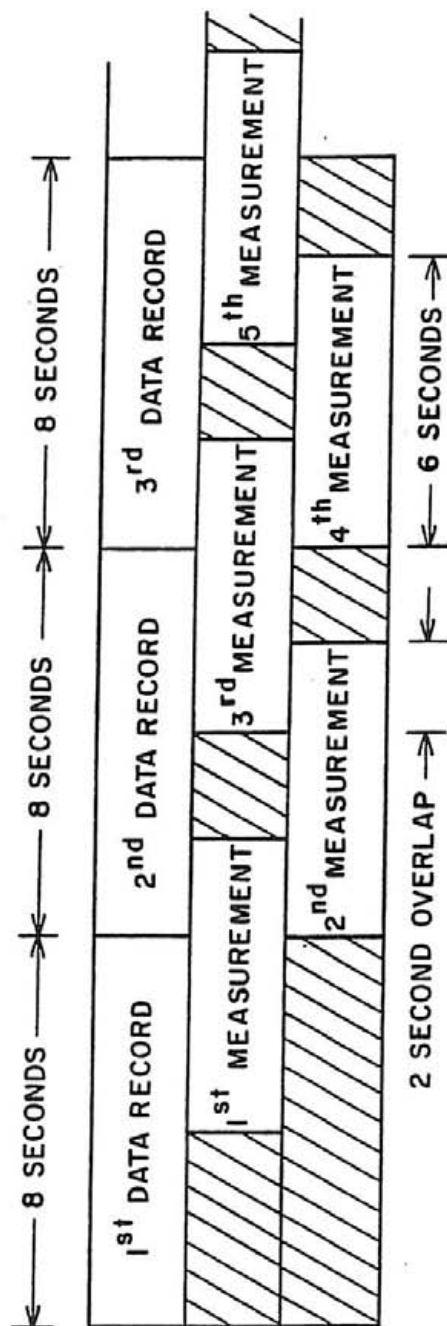


Figure 3

Figure 4 Graph of electric field data after computer processing. The data covers a time period of 80 minutes. The top plot shows the average Z axis electric field. Below that is the standard deviation calculated for each average value of E_z . The next two plots show the components of the spin plane electric field perpendicular and parallel to the magnetic field in the spin plane. The bottom plot is the chi error coefficient for the spin plane measurements.

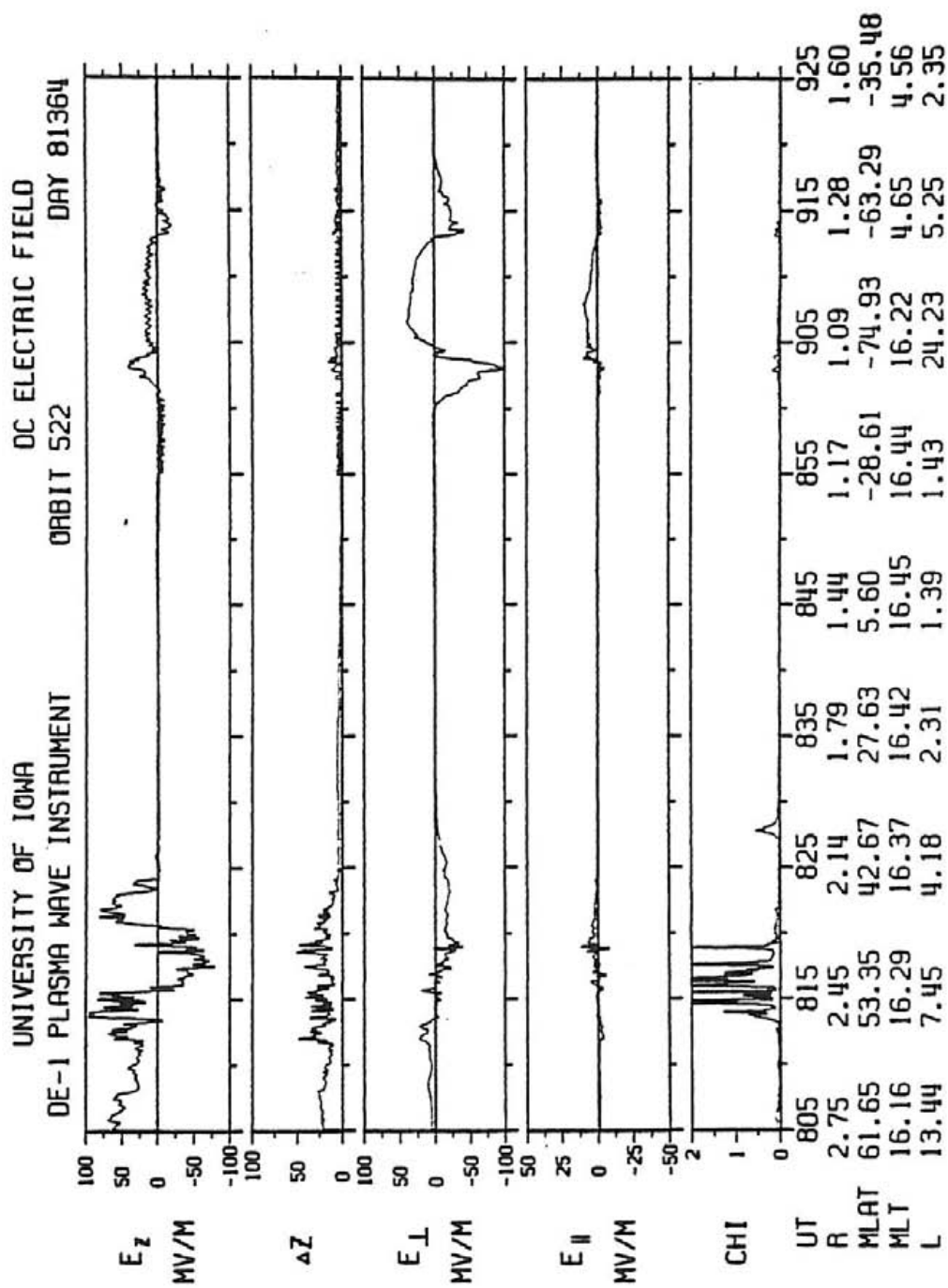


Figure 4

Figure 5

Diagram of the orientation of the E_1 electric field at different positions of the DE-1 spacecraft in its orbit. The calculation of E_1 is carried out in a spacecraft coordinate system, with axes \hat{X} , \hat{Y} , and \hat{Z} pointing in the direction shown. The \hat{Y} axis is defined to point toward the center of the earth. Since \underline{B} changes direction as the spacecraft orbits, the orientation of a positive E_1 also changes. In the northern hemisphere, a positive E_1 is in the direction of spacecraft motion, but is oppositely directed in the southern hemisphere. This diagram is highly simplified; the real orbit of DE-1 is elliptical.

A-G83-247

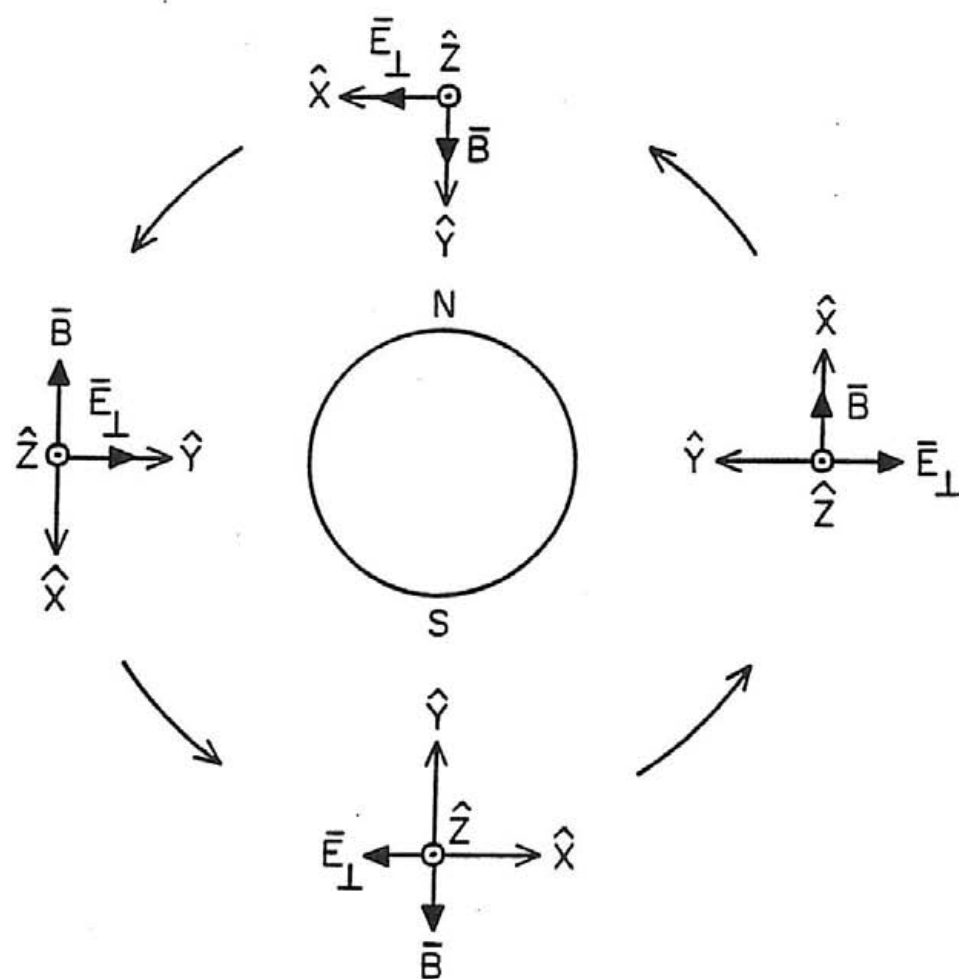


Figure 5

Figure 6

Illustration of a case when the magnetic field is not entirely in the spin plane. An electric field vector perpendicular to the magnetic field has a component in the spin plane labeled \underline{E}_{sp} . This vector may have a component parallel to the projection of the magnetic field into the spin plane. If \underline{B} lies completely in the spin plane, this situation cannot occur.

A-G83-173

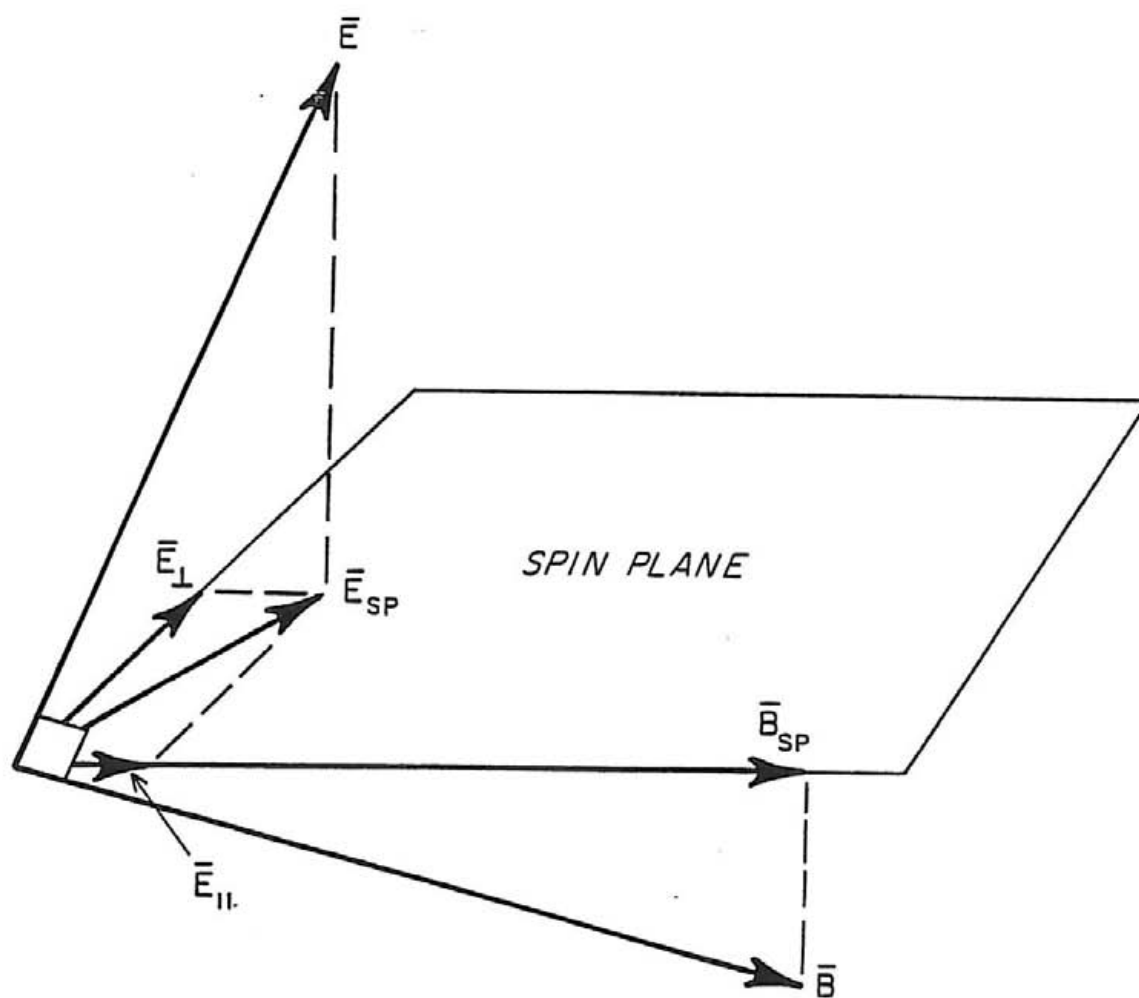


Figure 6

Figure 7

Peak electric field summary plot. This graph shows the peak electric fields, both positive and negative, measured on the z-axis and x-axis in each 6 second period. The plot also contains the calculated $\underline{V} \times \underline{B}$ electric field for both axes. The time period for this graph is the same as the graph in Figure 4. This type of graph is very useful for spotting large peaks in the electric field which get filtered out by the analysis program. The spike near 8:19 UT is one such case. The change in the digital resolution for the low-gain amplifier is evident at 9:02 UT.

A-G83-295

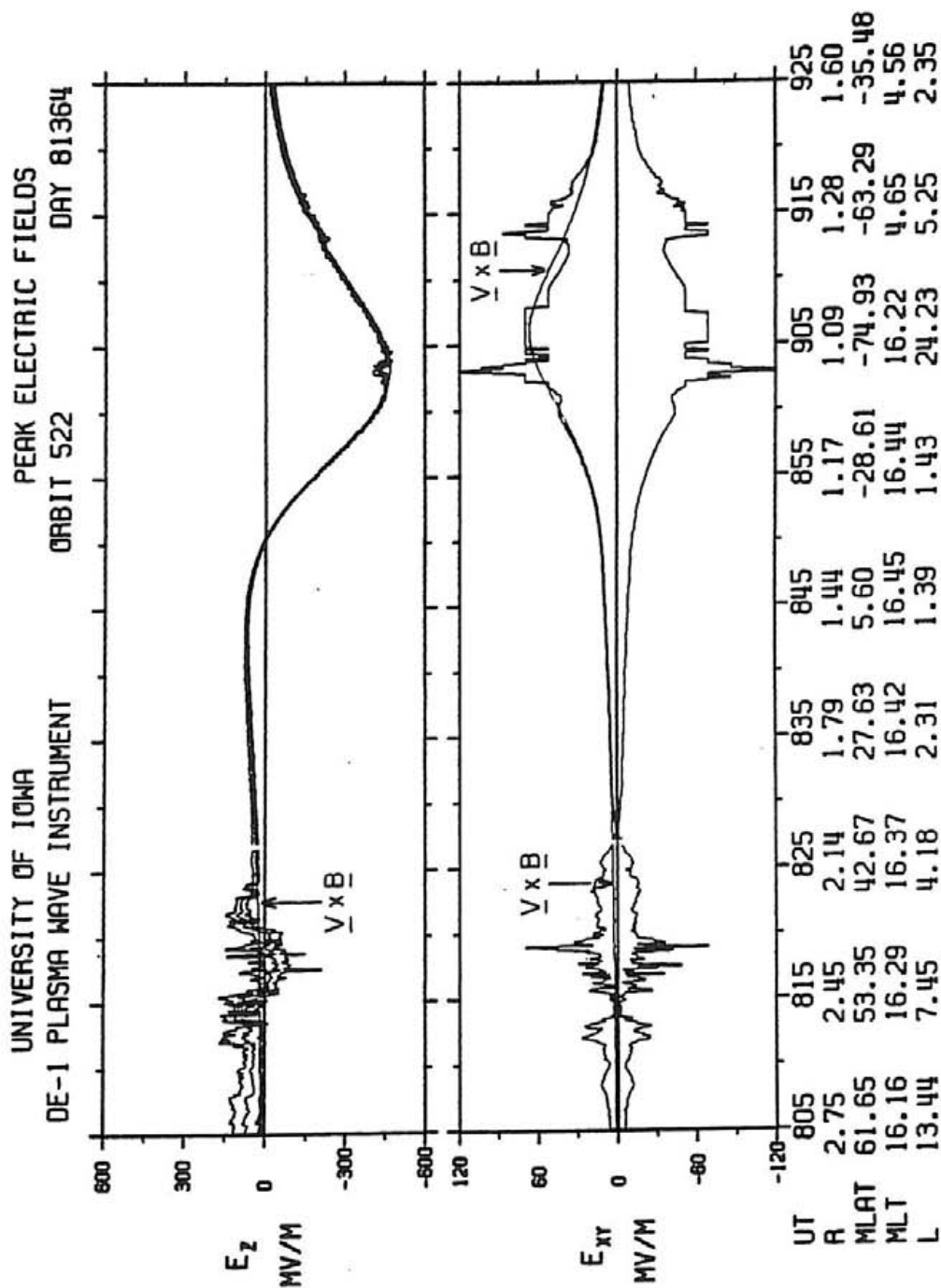


Figure 7

Figure 8 Southern hemisphere plasma convection measured from
6:15 UT to 6:39 UT on day 81343 (December 9, 1981).

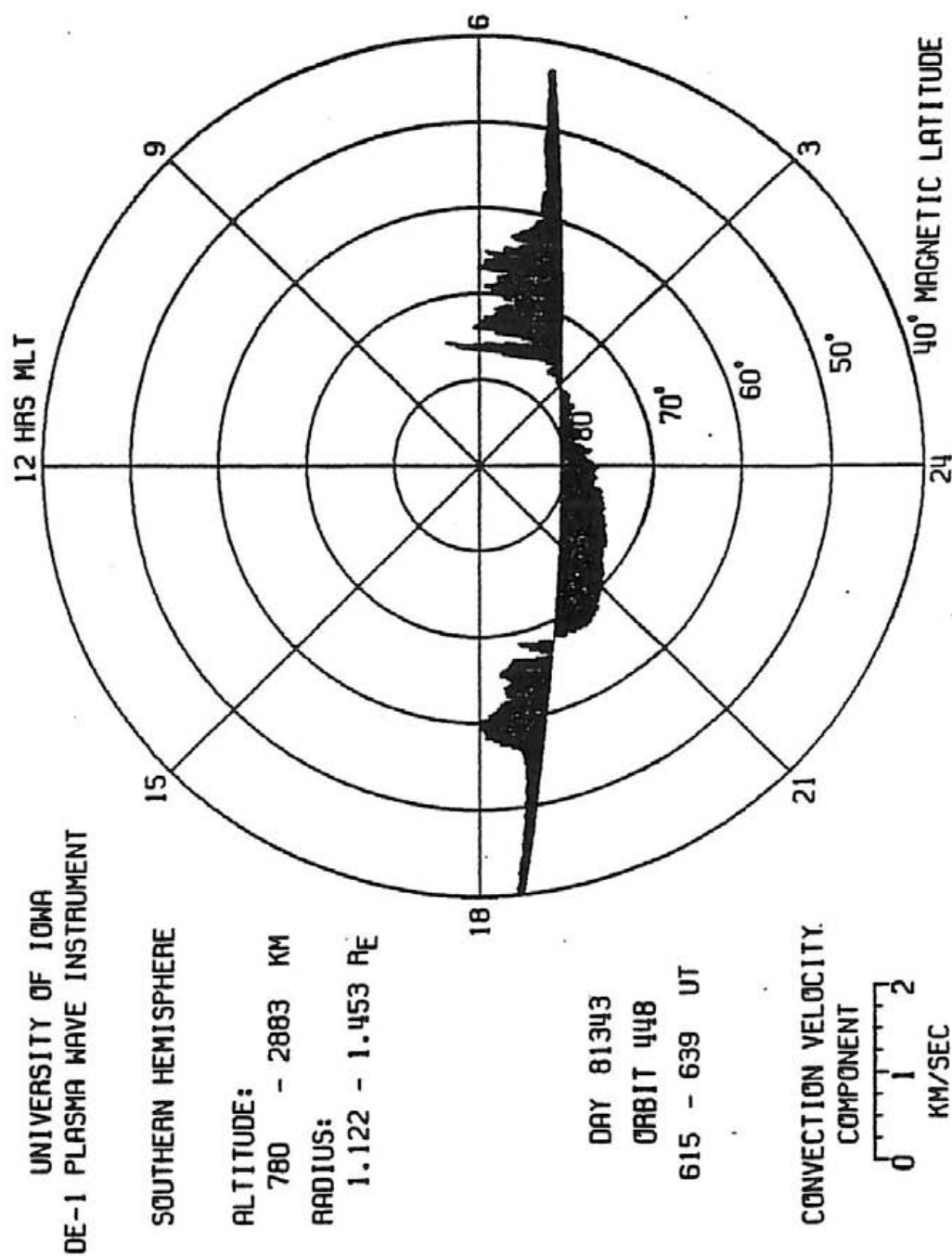


Figure 8

Figure 9 Empirical models of polar cap potentials derived by Heppner to match patterns in the OGO-6 data. Model A is a "sun-aligned" representation with 4 kV contour intervals corresponding to the standard two-cell pattern. Model B shows a mode of distorting the two-cell pattern to account for regions of reverse flow in the 18-24 hours local time sector.

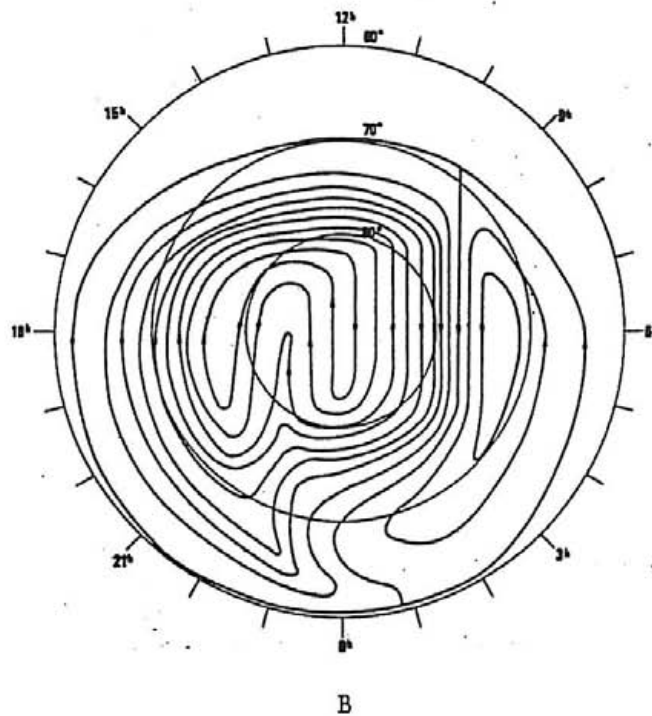
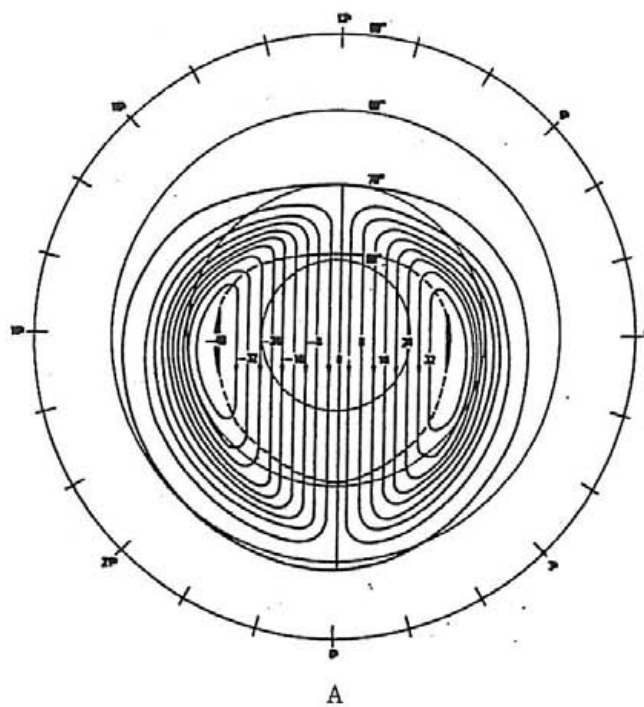


Figure 9

Figure 10

Interplanetary magnetic field data and geomagnetic activity indices for day 81343 (December 9, 1981). The bar after 6 hours marks the period when the data in figure 8 was obtained. Just before this time, the IMF was southward (negative B_z). The IMF data was obtained from the National Space Science Data Center composite omnitape SM-41B. The magnetic activity indices are from Solar Geophysical Data, published by NOAA Environmental Data and Information Service.

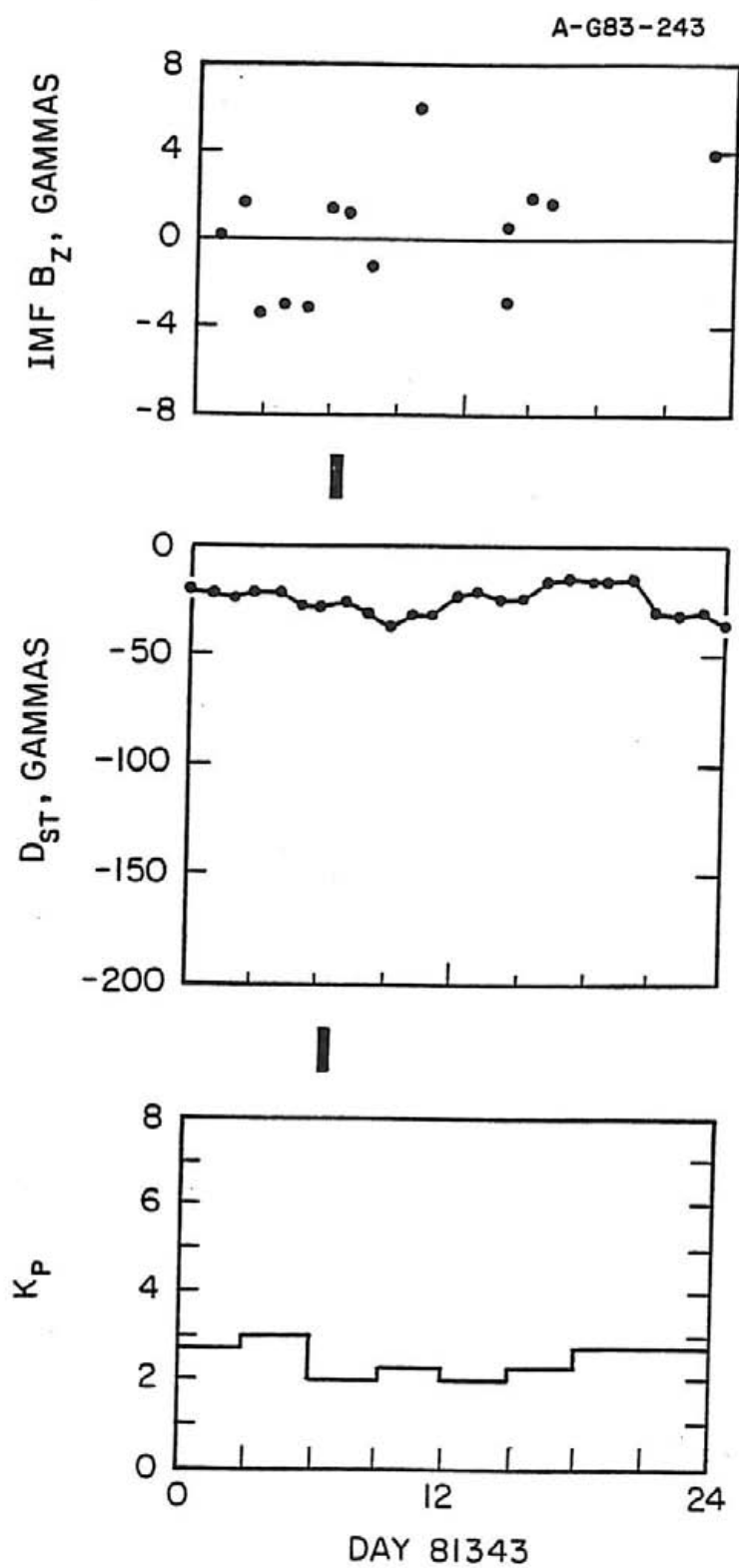


Figure 10

Figure 11 Southern hemisphere plasma convection measured from 8:06 UT to 8:29 UT on day 81287 (October 14, 1981). This is the first of three graphs illustrating the variability from one orbit to the next. During this time DE-1 was reaching perigee altitude of 675 km over the south pole. The altitudes in the figure refer to the start and end points on the plot.

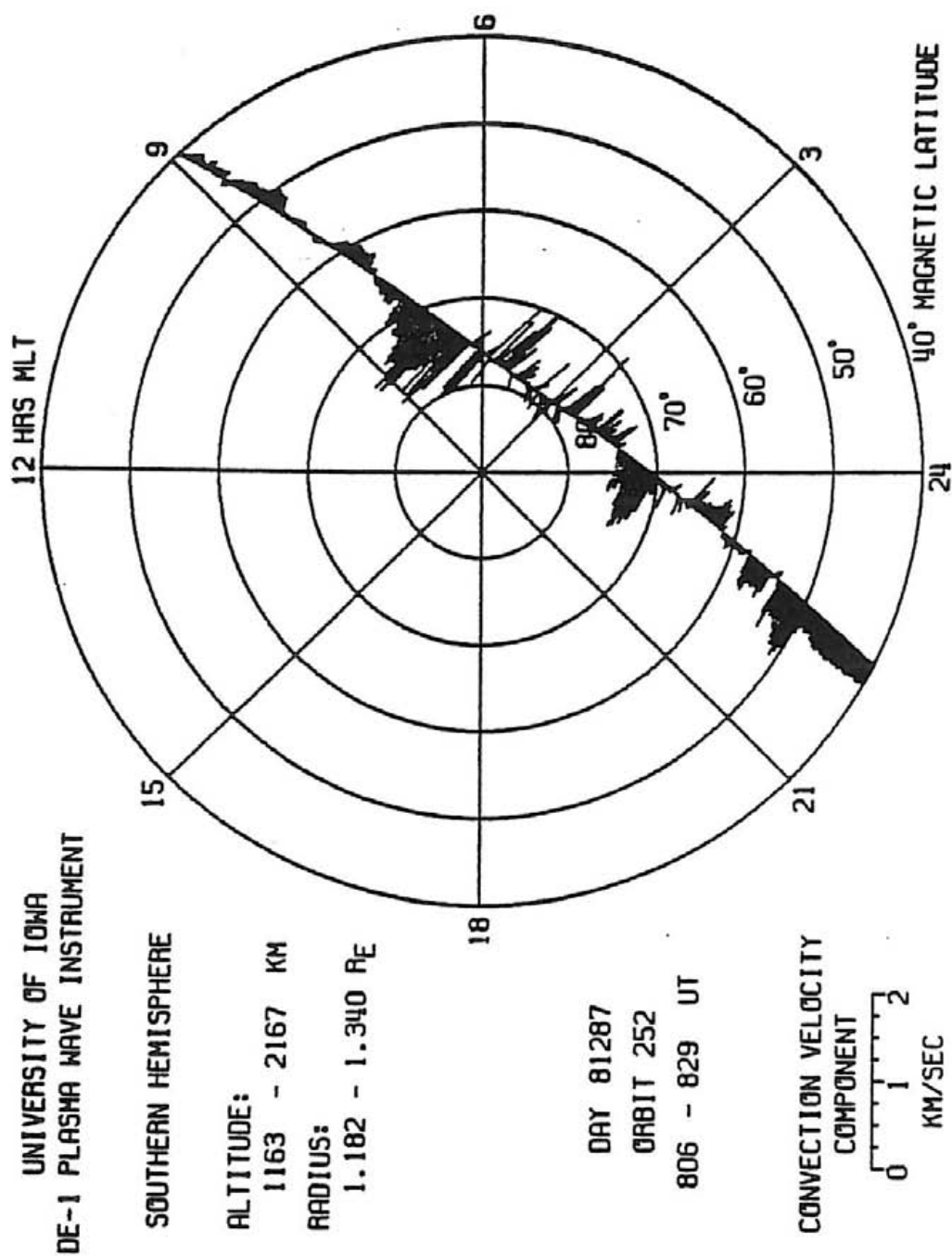


Figure 11

Figure 12 Southern hemisphere plasma convection measured from
14:54 UT to 15:17 UT on day 81287 (October 14, 1981).

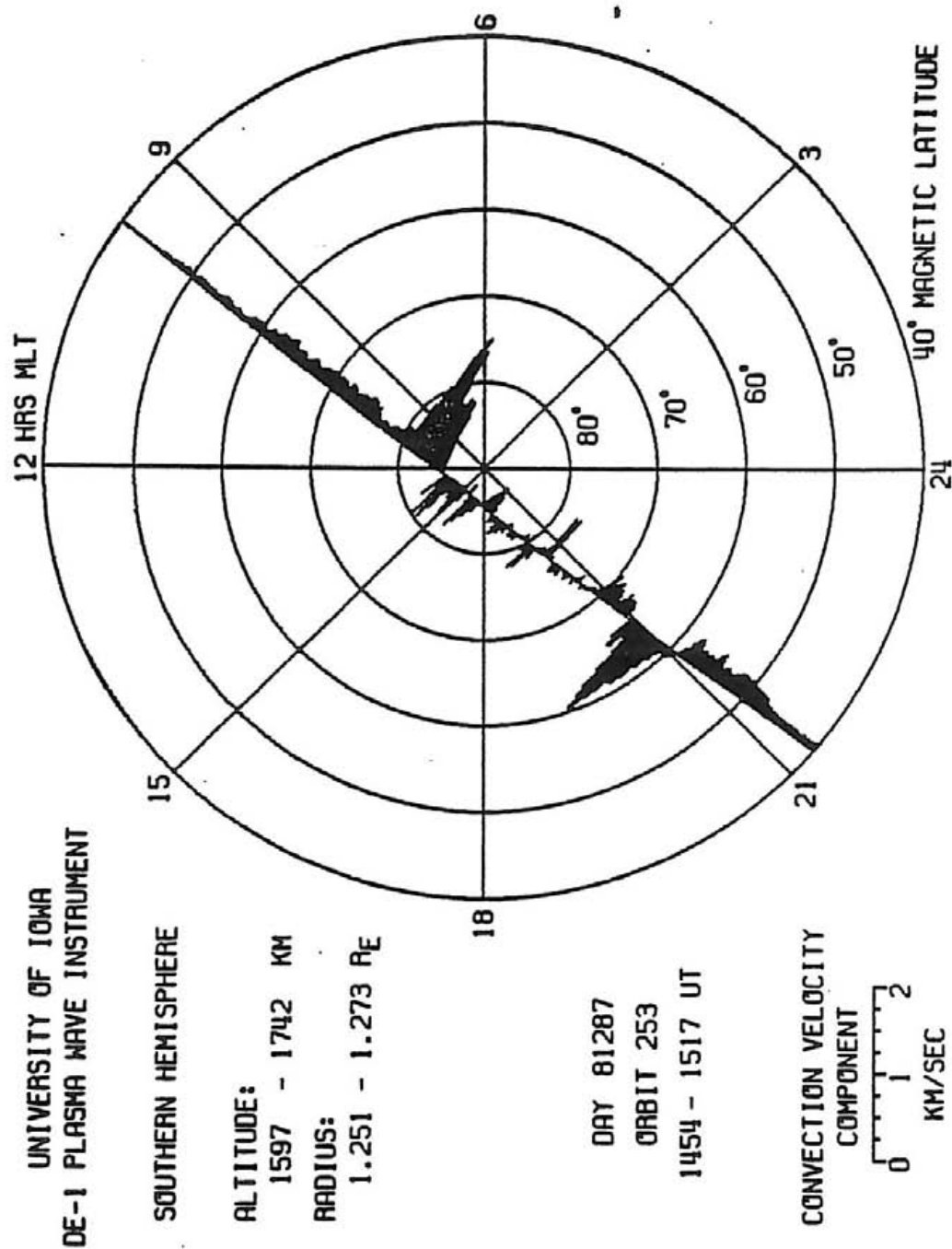


Figure 12

Figure 13

Southern hemisphere plasma convection measured from 21:49 UT to 22:14 UT on day 81287 (October 14, 1981). There is a gap in the data from 60° to 65° MLAT in the morning sector.

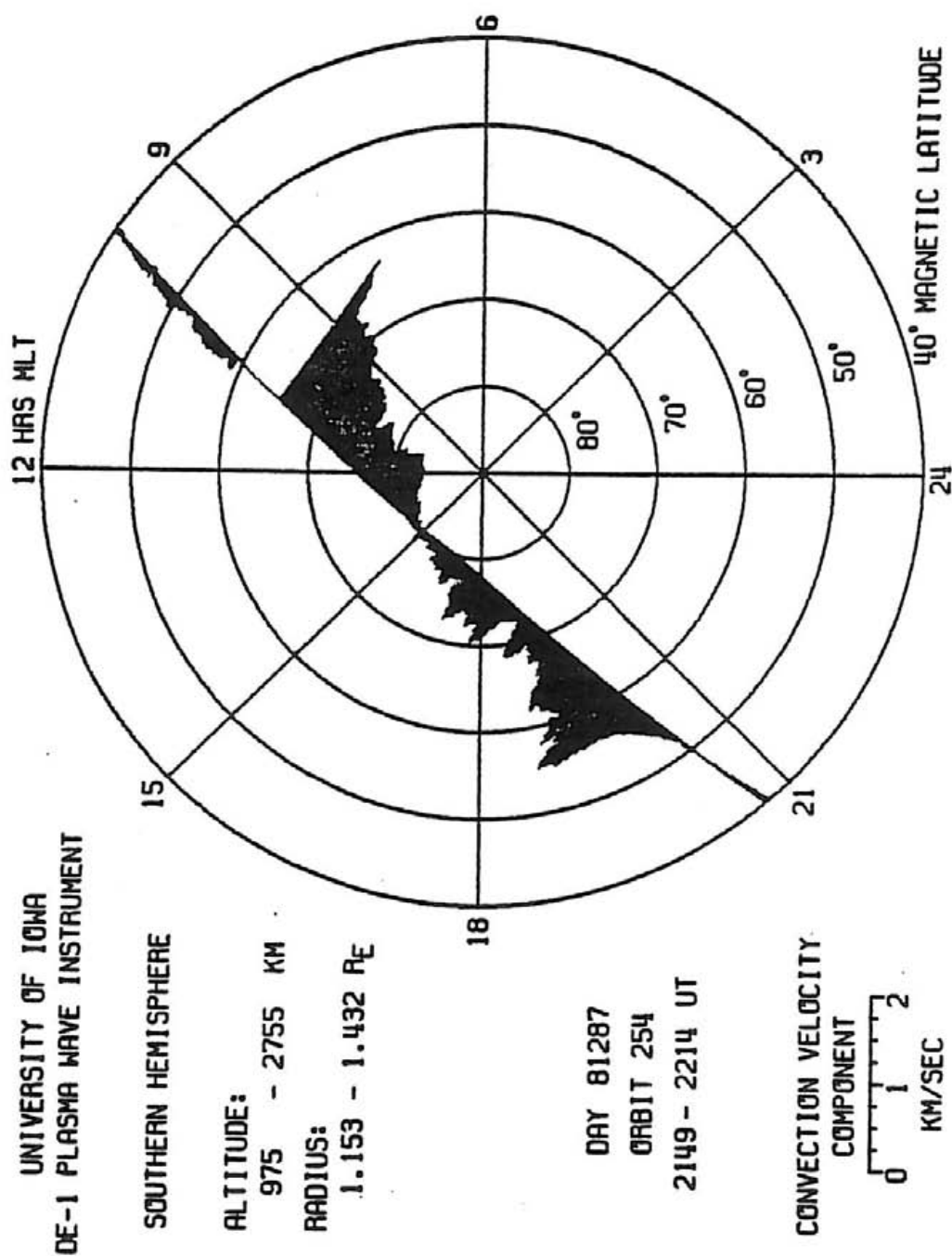


Figure 13

Figure 14 Interplanetary magnetic field and geomagnetic activity indices for day 81287 (October 14, 1981). The three dark bars mark the periods when the data in figures 11, 12, and 13 were obtained.

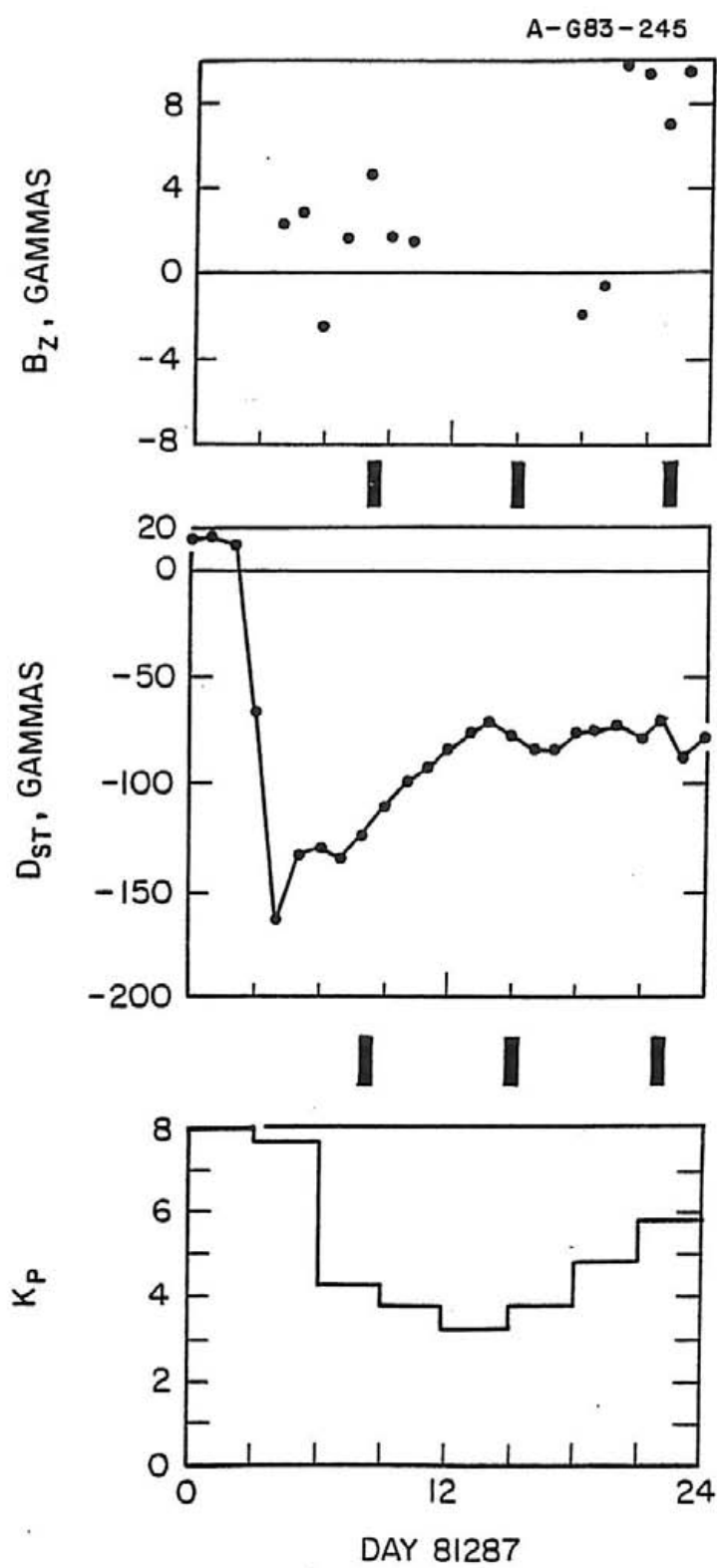


Figure 14

Figure 15 Southern hemisphere plasma convection measured from
4:29 UT to 4:53 UT on day 81294 (October 21, 1981).

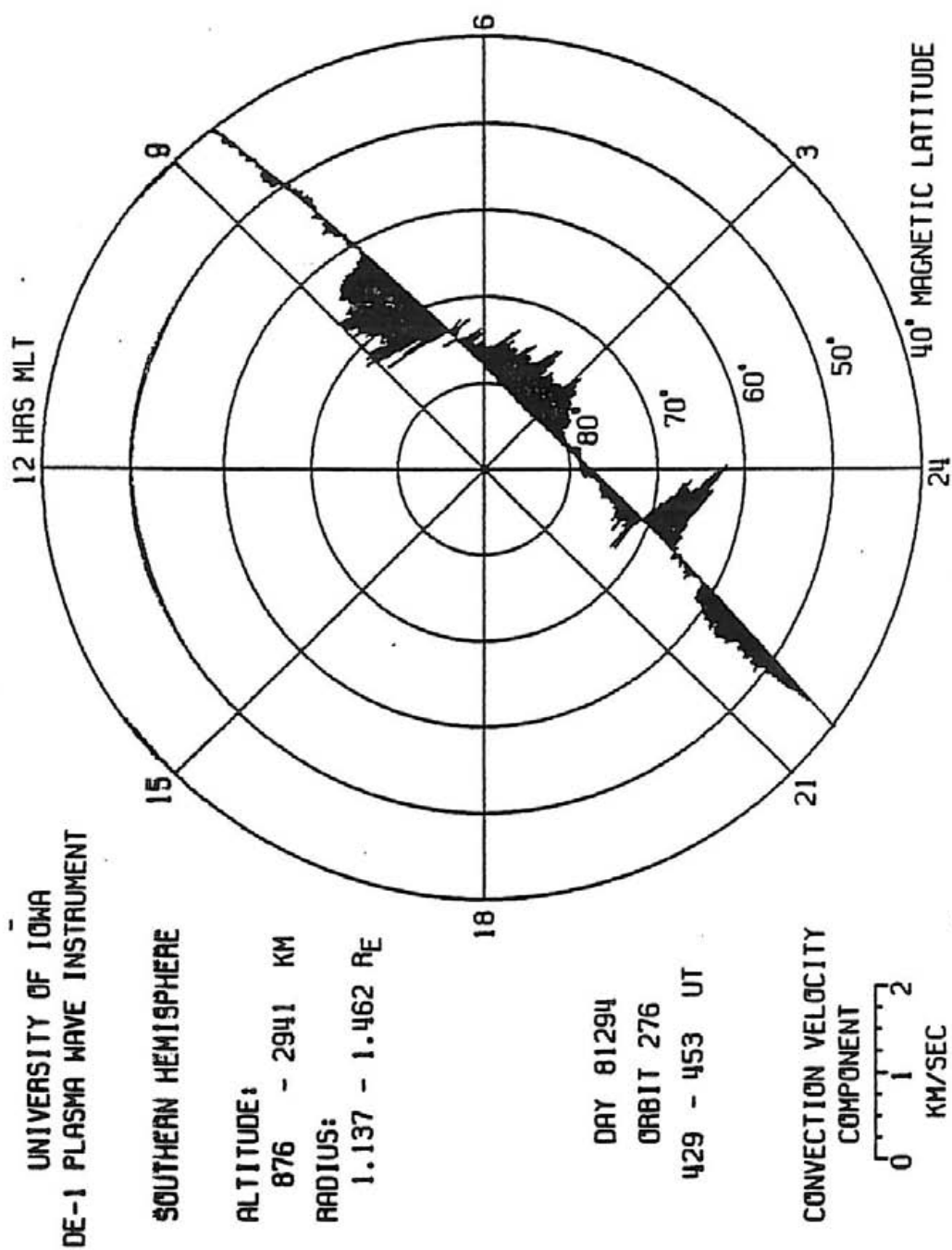


Figure 15

Figure 16 Southern hemisphere plasma convection measured from
11:16 UT to 11:39 UT day 81294 (October 21, 1981).

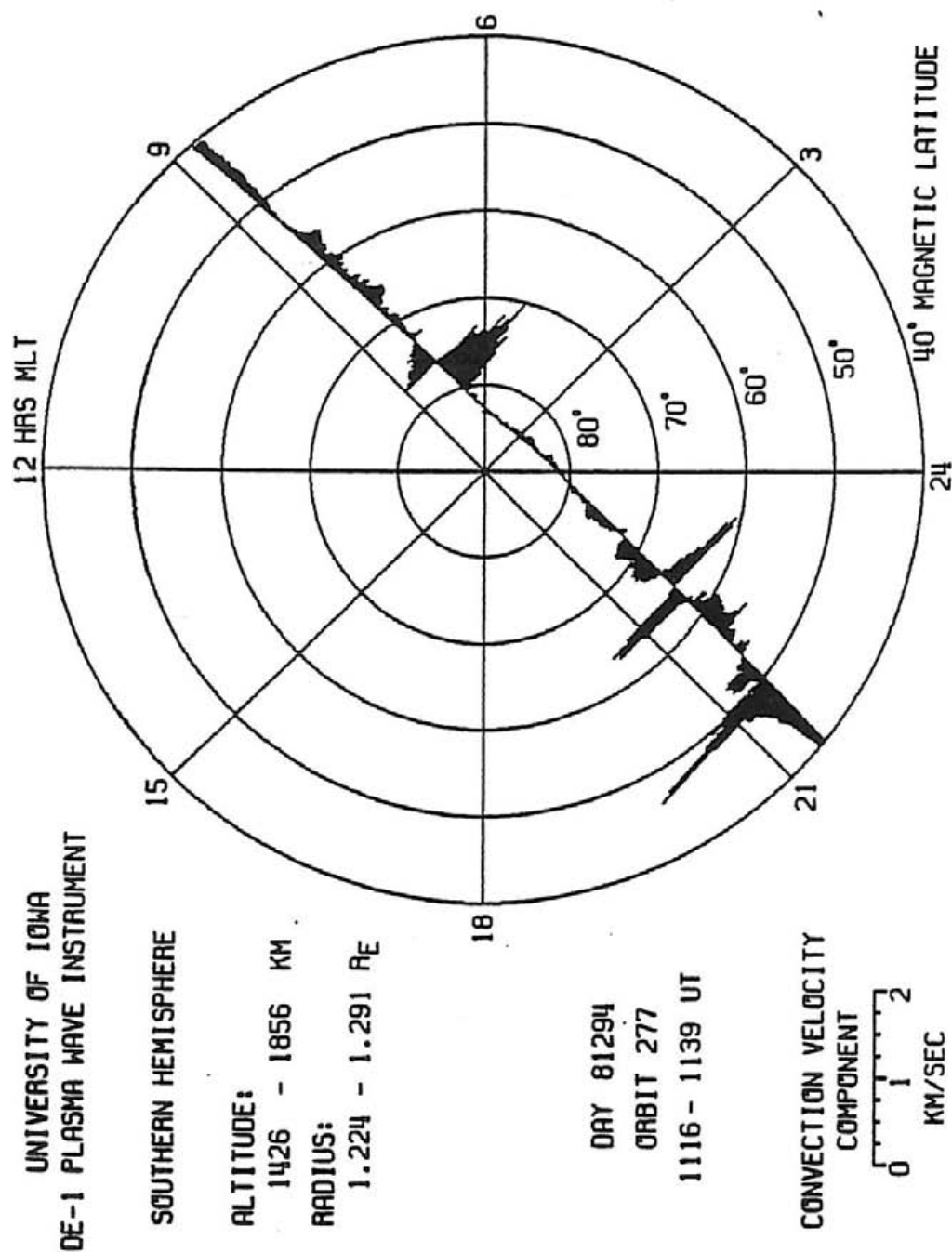


Figure 16

Figure 17 Southern hemisphere plasma convection measured from
18:08 UT to 18:32 UT day 81294 (October 21, 1981).
There is a gap in the transmitted data around 15 hrs.
MLT.

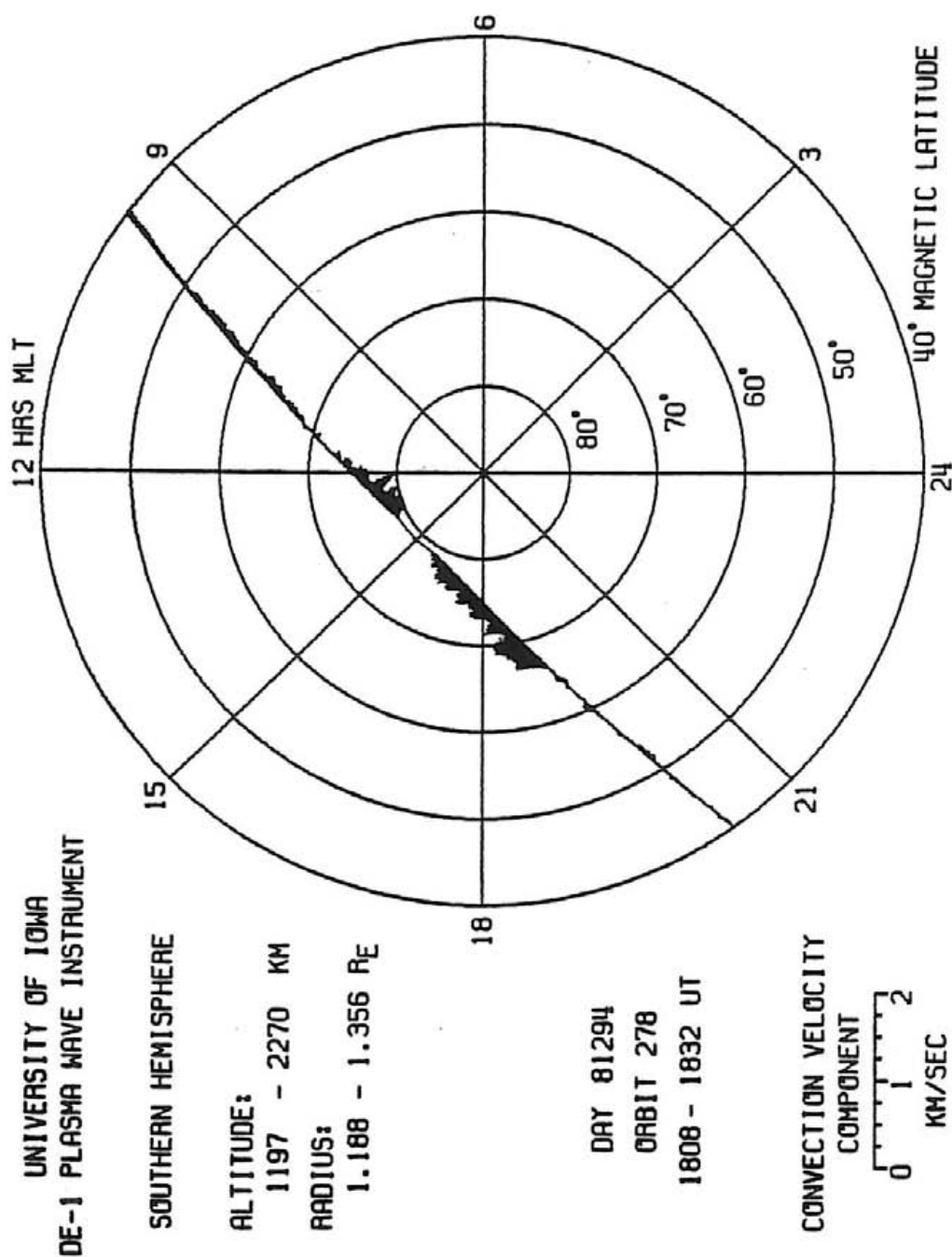


Figure 17

Figure 18

Southern hemisphere plasma convection measured from
1:03 UT to 1:28 UT day 81295 (October 22, 1981).

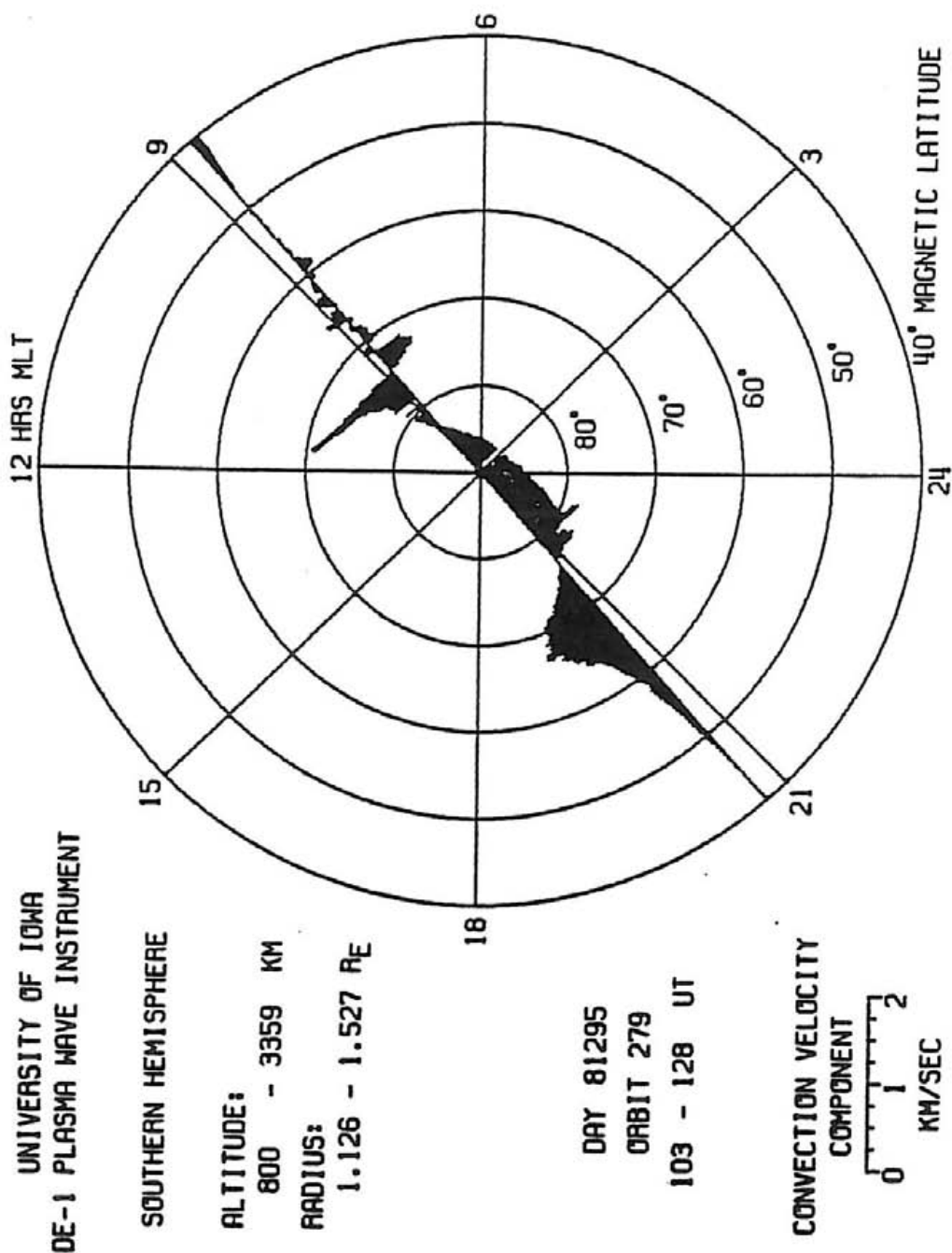


Figure 18

Figure 19 Southern hemisphere plasma convection measured from
4:25 UT to 4:50 UT day 81296 (October 23, 1981).

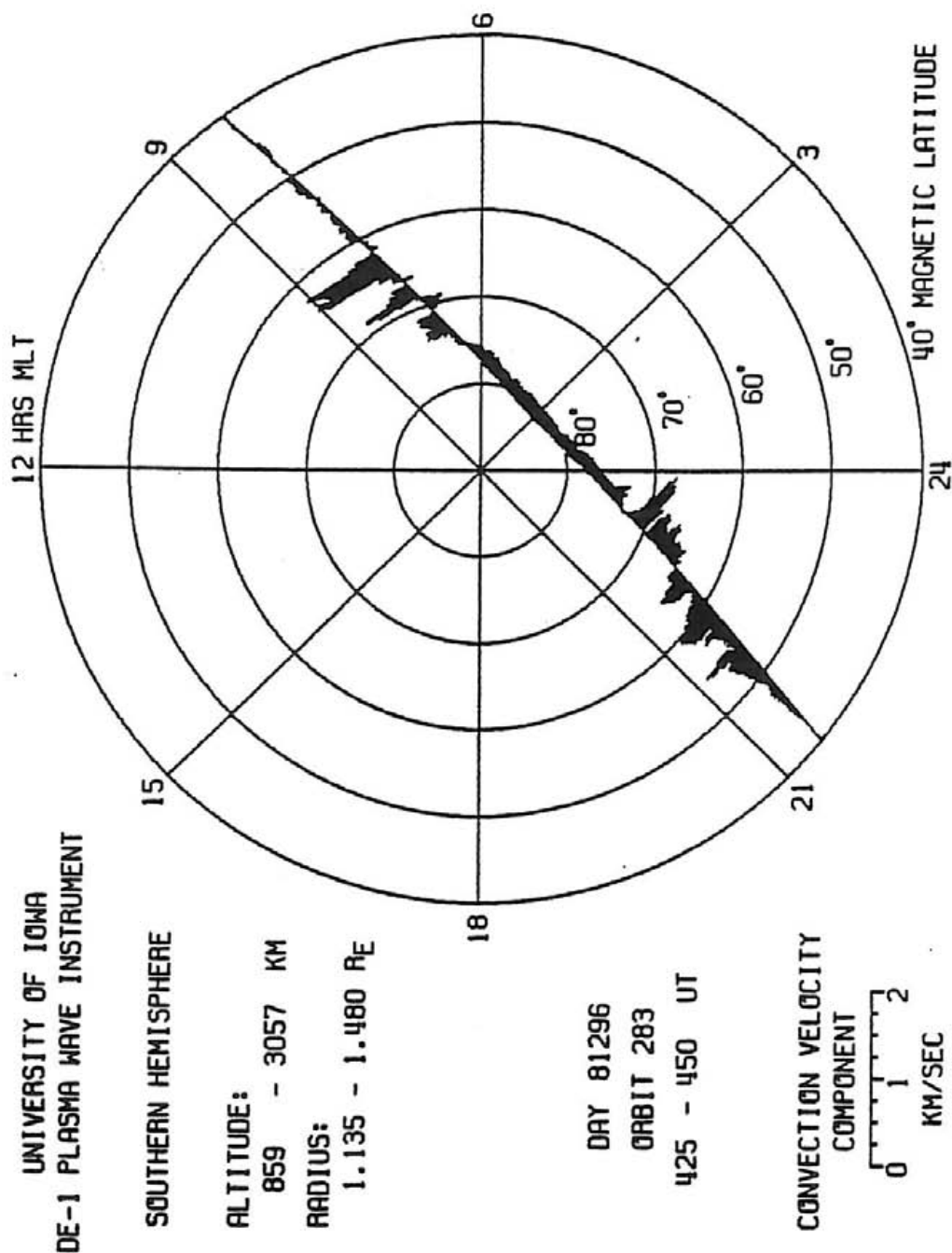


Figure 19

Figure 20 Southern hemisphere plasma convection measured from
11:12 UT to 11:35 UT day 18296 (October 23, 1981).

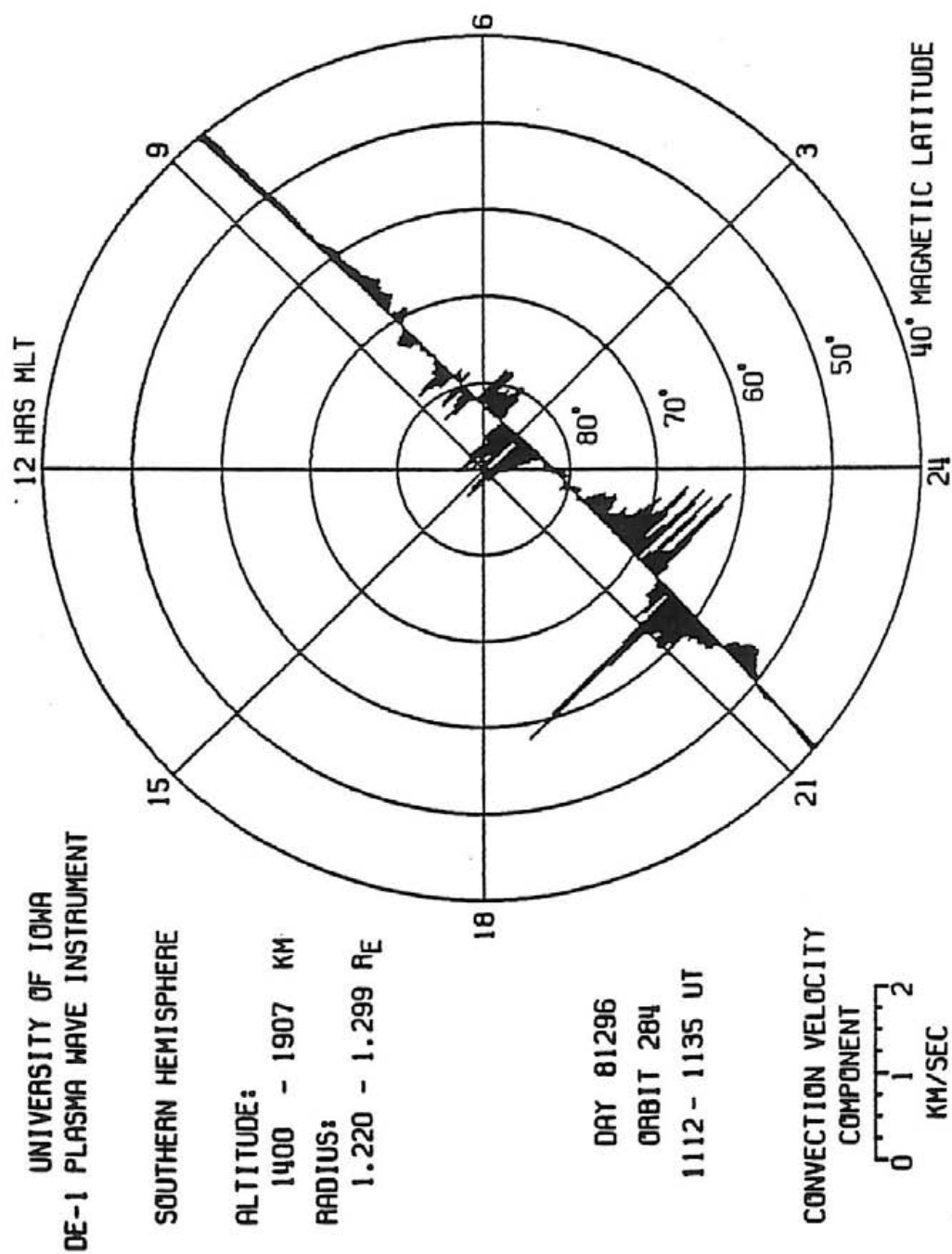


Figure 20

Figure 21 Southern hemisphere plasma convection measured from
4:22 UT to 4:46 UT day 81298 (October 25, 1981).

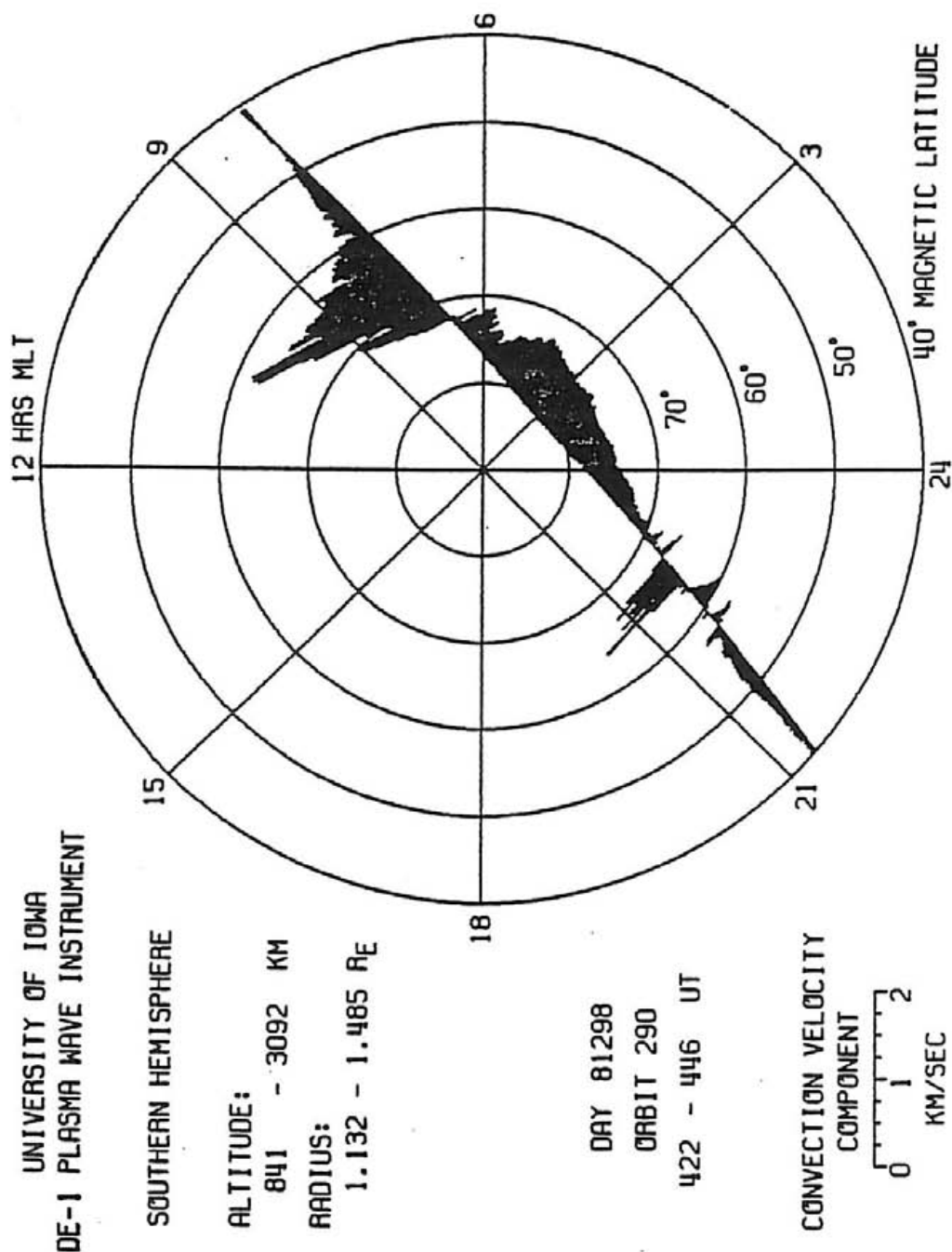


Figure 21

Figure 22 Geomagnetic activity indices for the period from day 81294 (October 21, 1981) to day 81298 (October 25, 1981). The seven bars positioned along the time scale mark the periods when the data on figures 15 through 21 were obtained.

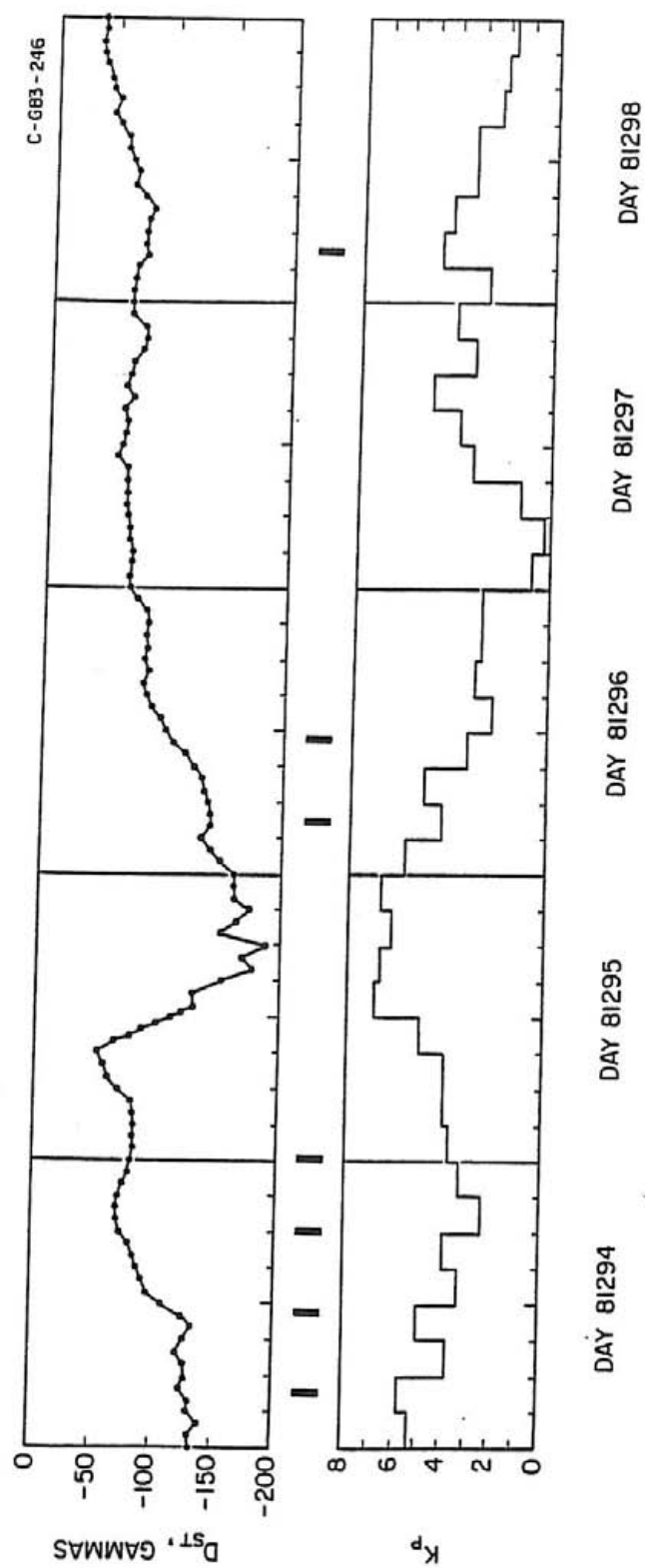


Figure 22

Figure 23 Southern hemisphere plasma convection measured from 8:57 UT to 9:23 UT on day 81364 (December 30, 1981). This graph has the best plasma flow pattern corresponding to a two-cell circulation seen in the data processed to date. The electric field graphs for this time period are in Figures 4 and 7.

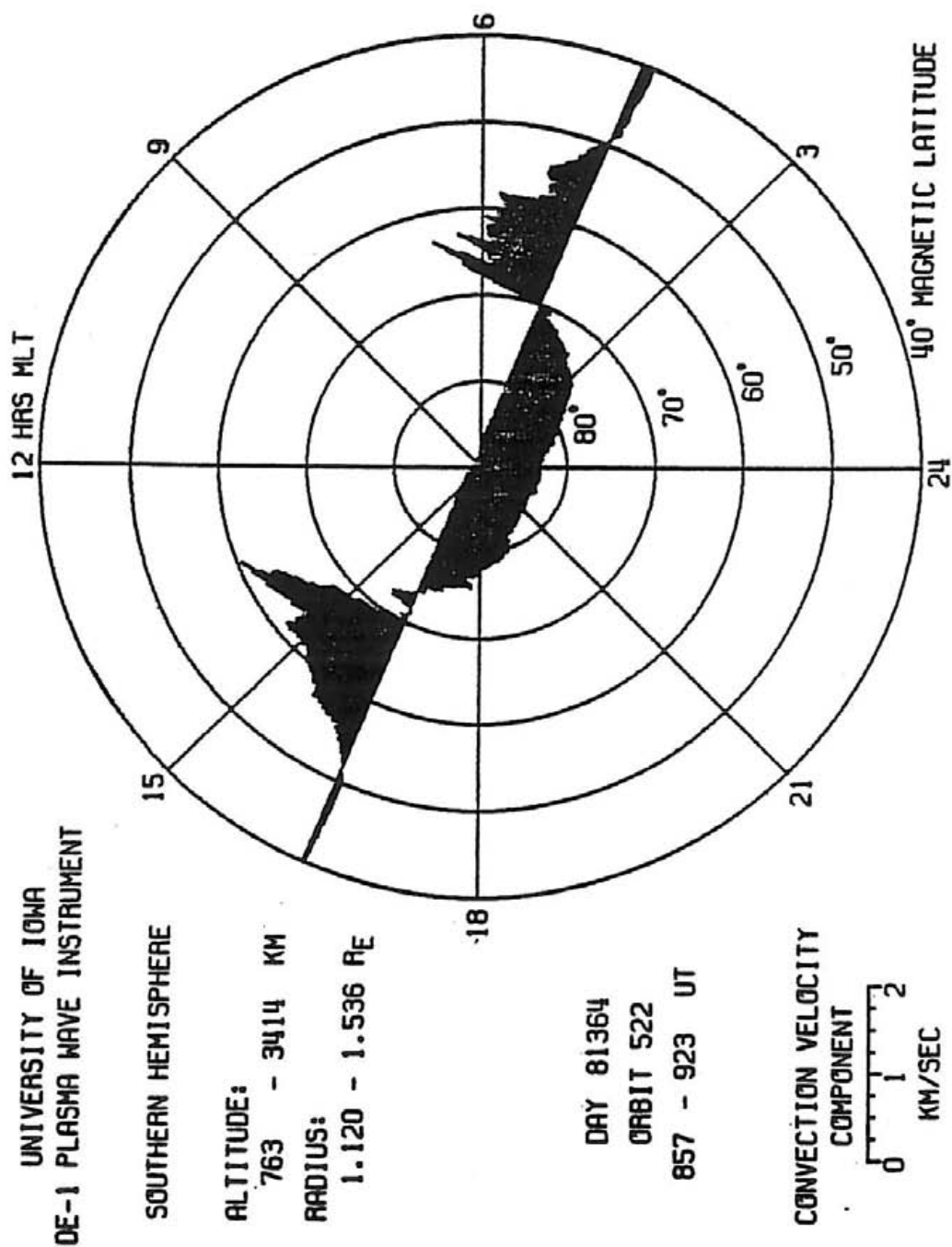


Figure 23

Figure 24 Interplanetary magnetic field data and geomagnetic activity indices for day 81364 (December 30, 1981). The bar on the time scale marks the time when the data in figure 23 were obtained.

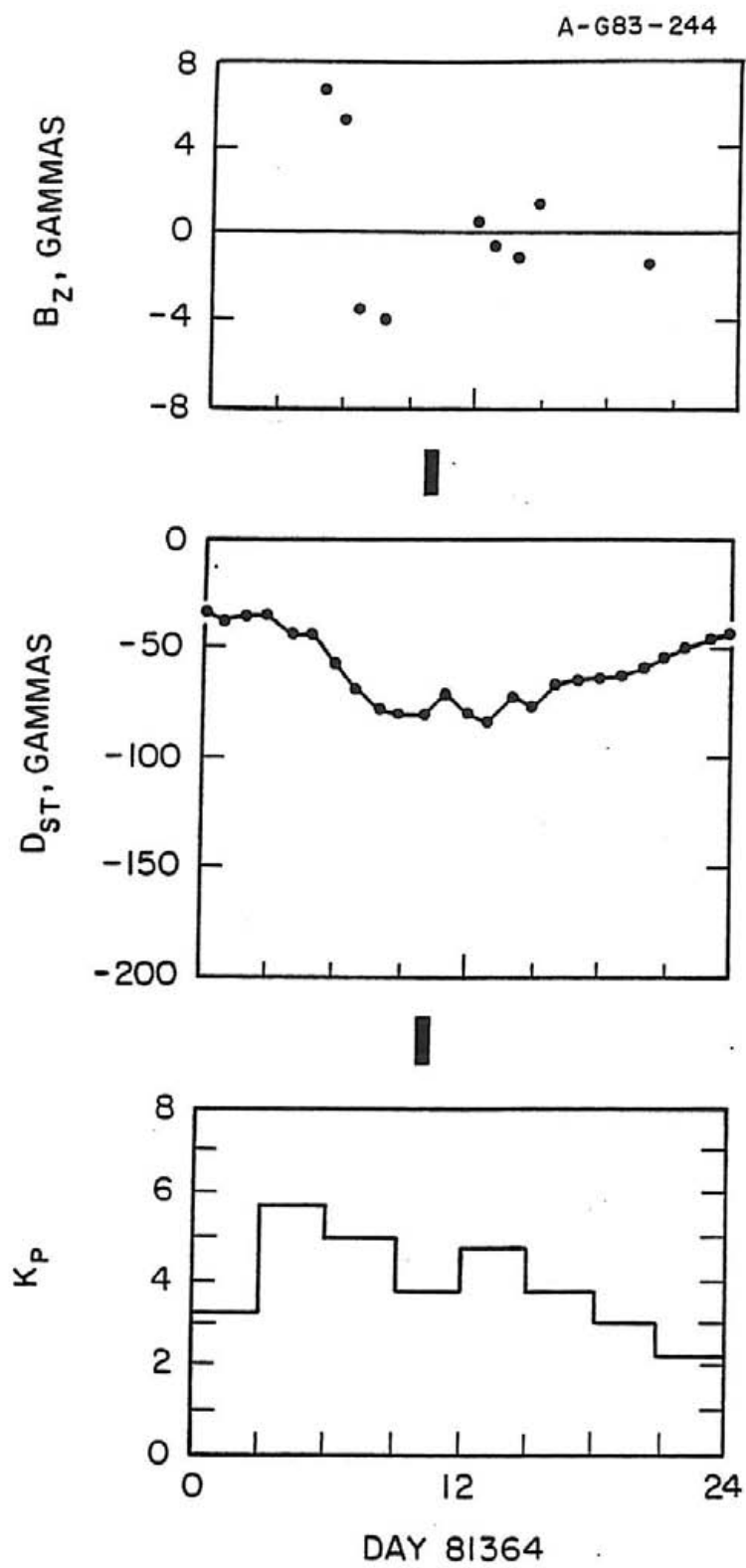


Figure 24

Figure 25

Example of oppositely directed electric fields detected on auroral field lines. The DE-1 spacecraft was at an invariant latitude of 65.3° and altitude of 9,000 km, moving 5.46 km/s. At 28 seconds from the start of the plot, a field with a magnitude of 90 mV/m was detected. In the next spin period a larger field was detected, but with a 180° phase reversal.

A-G83-293

UNIVERSITY OF IOWA
DE-1 PLASMA WAVE INSTRUMENT DC ELECTRIC FIELD
ORBIT 283 DAY 81296 UT 3:44:44 - 3:45:56

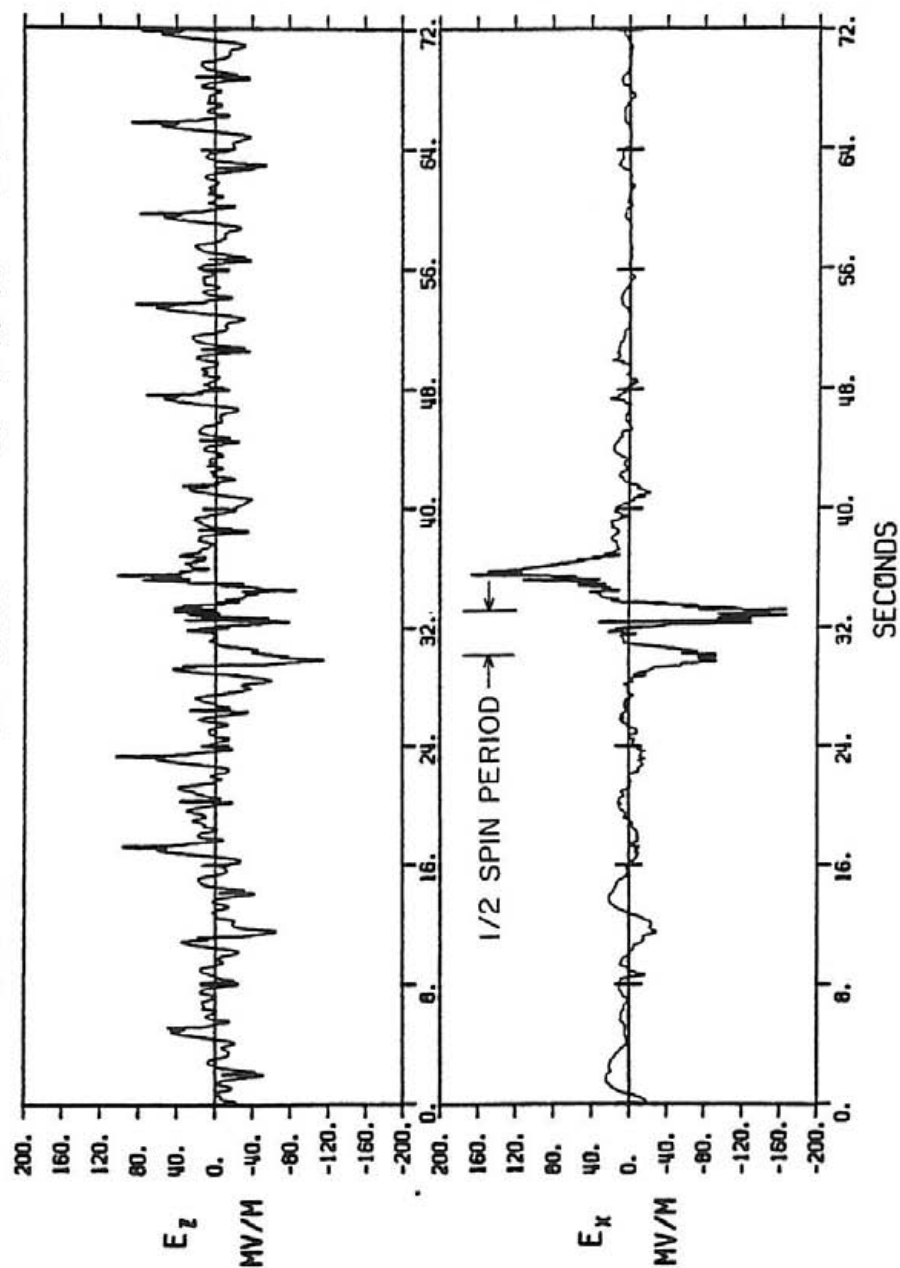


Figure 25

Figure 26 Northern hemisphere plasma convection measured from
14:35 UT to 15:35 UT on day 82092 (April 2, 1982).
At 15:27 UT an "auroral vortex" was encountered.

A-G83-296

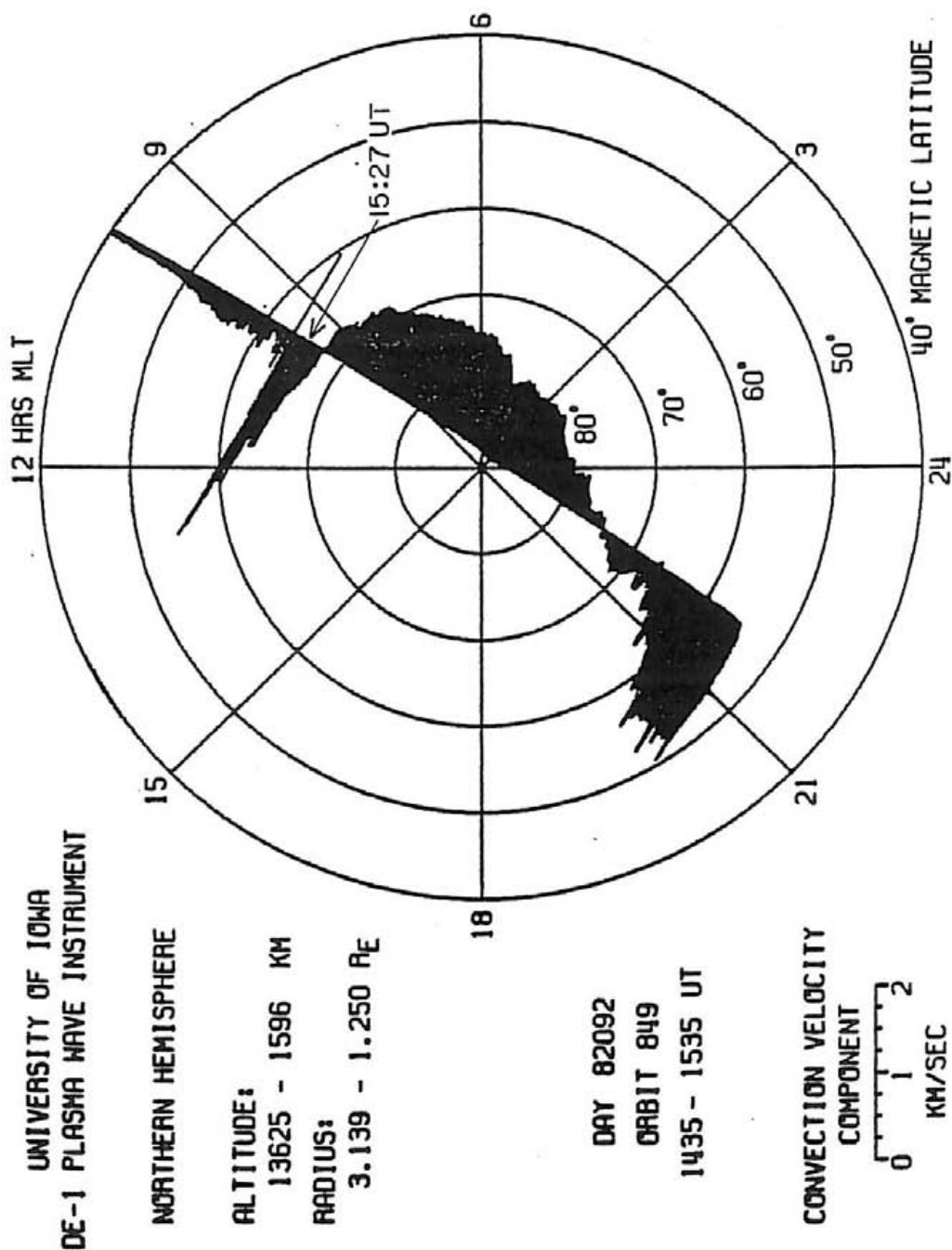


Figure 26

Figure 27

High-resolution electric field data for the auroral vortex event at 15:27 UT on day 82092. Up to the time 32 seconds from the start of the plot the field in the spin plane (E_x) is increasing, then there is a sudden reversal. The field at 35 seconds is 180° out of phase. After 44 seconds the phase of the sine wave is the same as at the start. A very large change is seen on the Z axis at the same point where the field in the spin plane reverses.

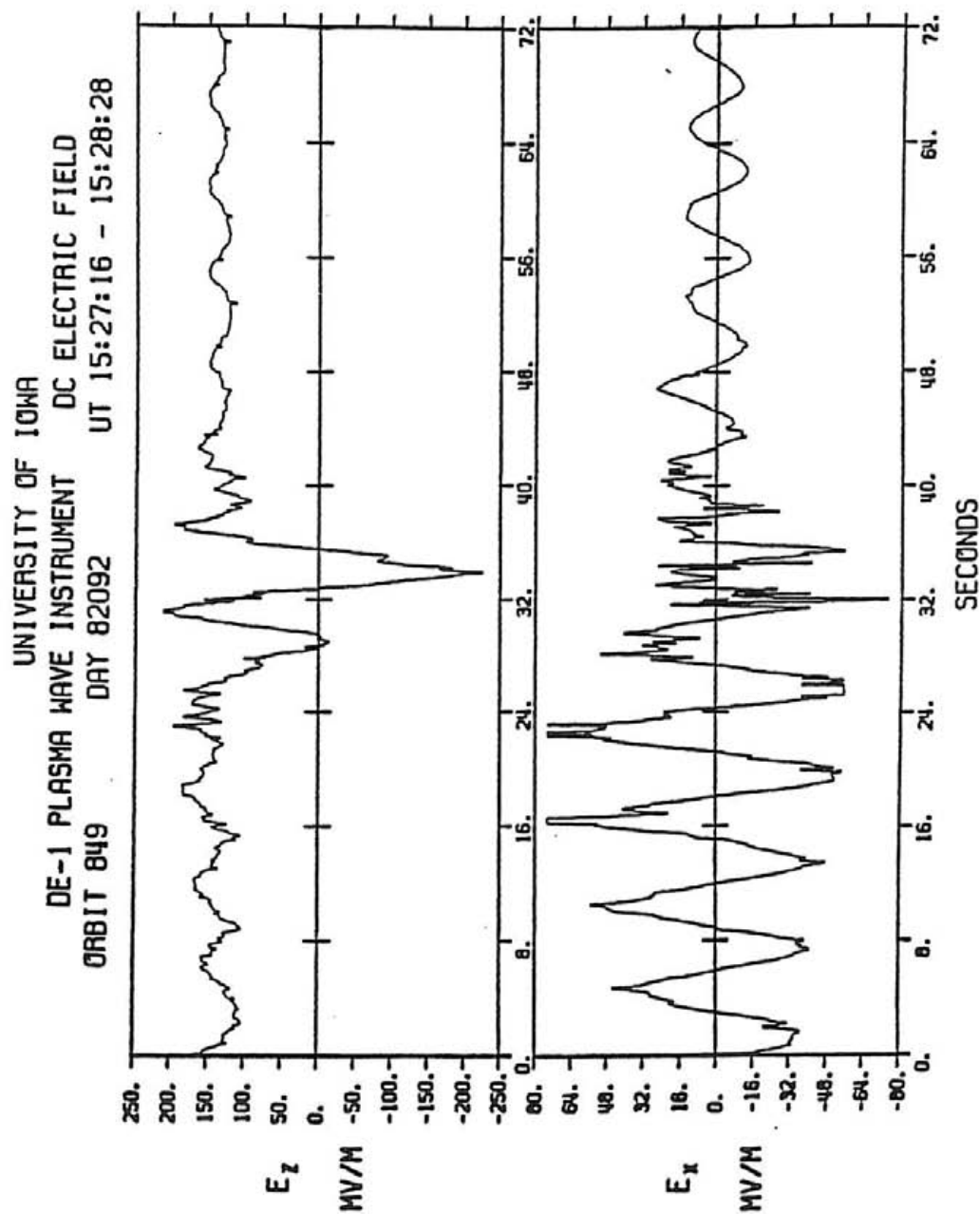


Figure 27

Figure 28 Plasma Wave Instrument spectrogram for 14:30 UT to 18:30 UT on day 82092 (April 2, 1982). A broadband noise burst was detected at 15:27 UT, coincident with the auroral vortex seen in the electric field data.

A-G83-292

UNIVERSITY OF IOWA DE-1 PLASMA WAVE INSTRUMENT
 SFRA EX DAY 92 APRIL 2, 1982 ORBIT 849

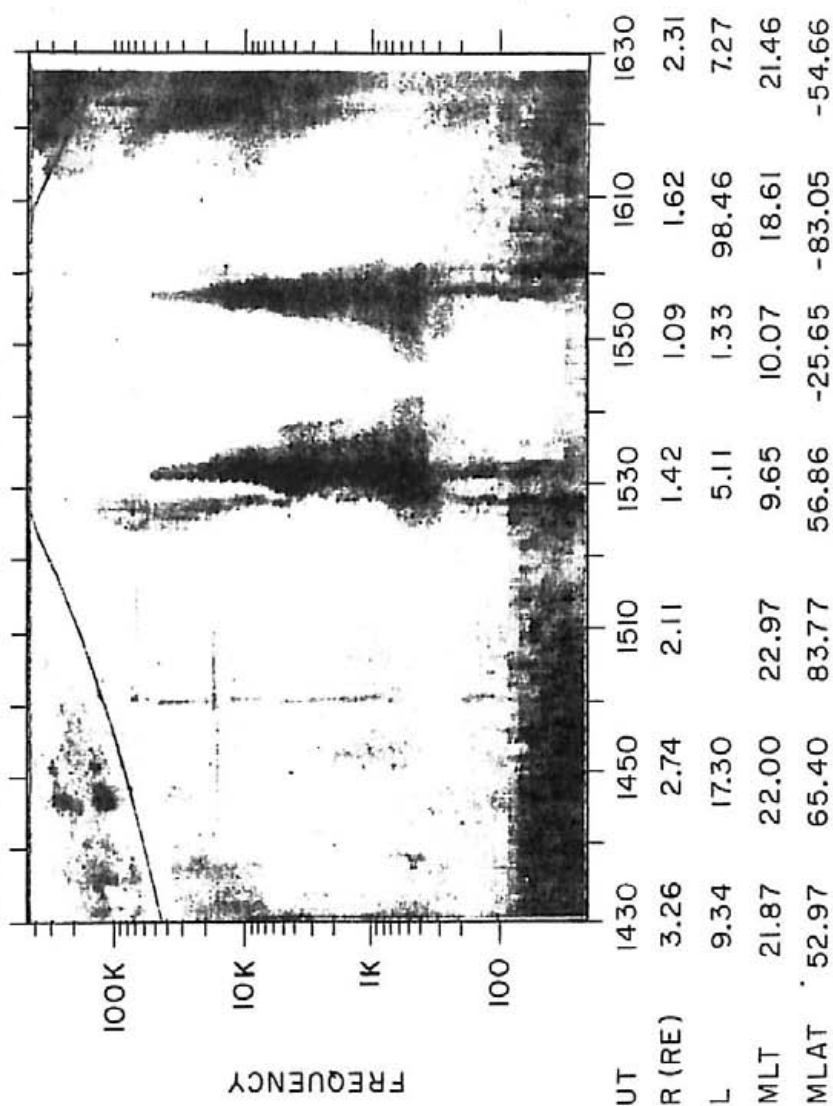


Figure 28

Figure 29 Southern hemisphere plasma convection measured from 22:02 UT to 22:43 UT on day 82108 (April 18, 1982). The events of interest are the peak at 22:09 UT and the sudden reversal at 22:24 UT.

A-G83-297

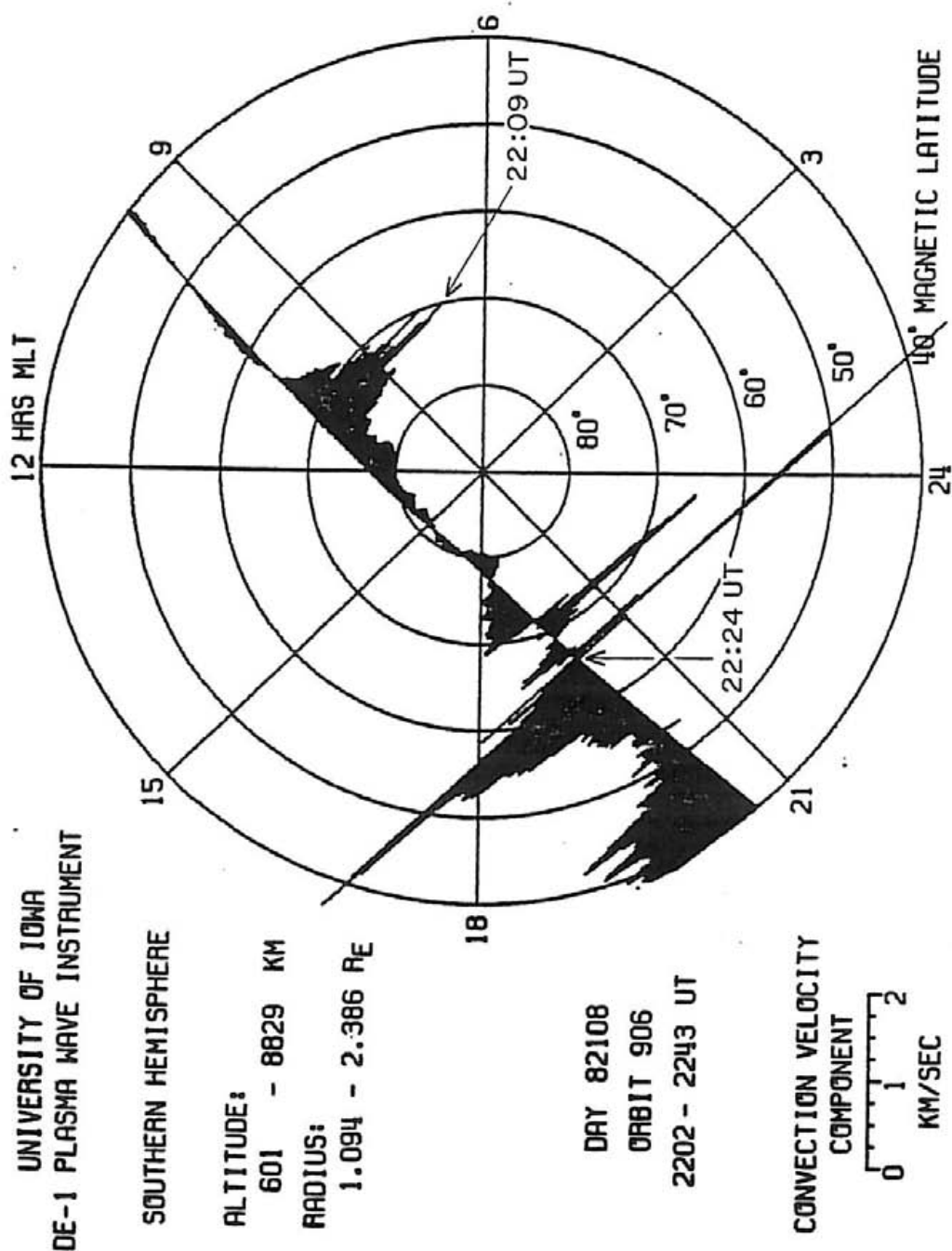


Figure 29

Figure 30 Plasma Wave Instrument spectrogram for 21:30 UT to
23:30 UT on day 82108 (April 18, 1982). Broadband
noise bursts occur at 22:09 UT and 22:24 UT.

A-G83-291

UNIVERSITY OF IOWA DE-1 PLASMA WAVE INSTRUMENT
 SFRA EX DAY 108 APRIL 18, 1982 ORBIT 906

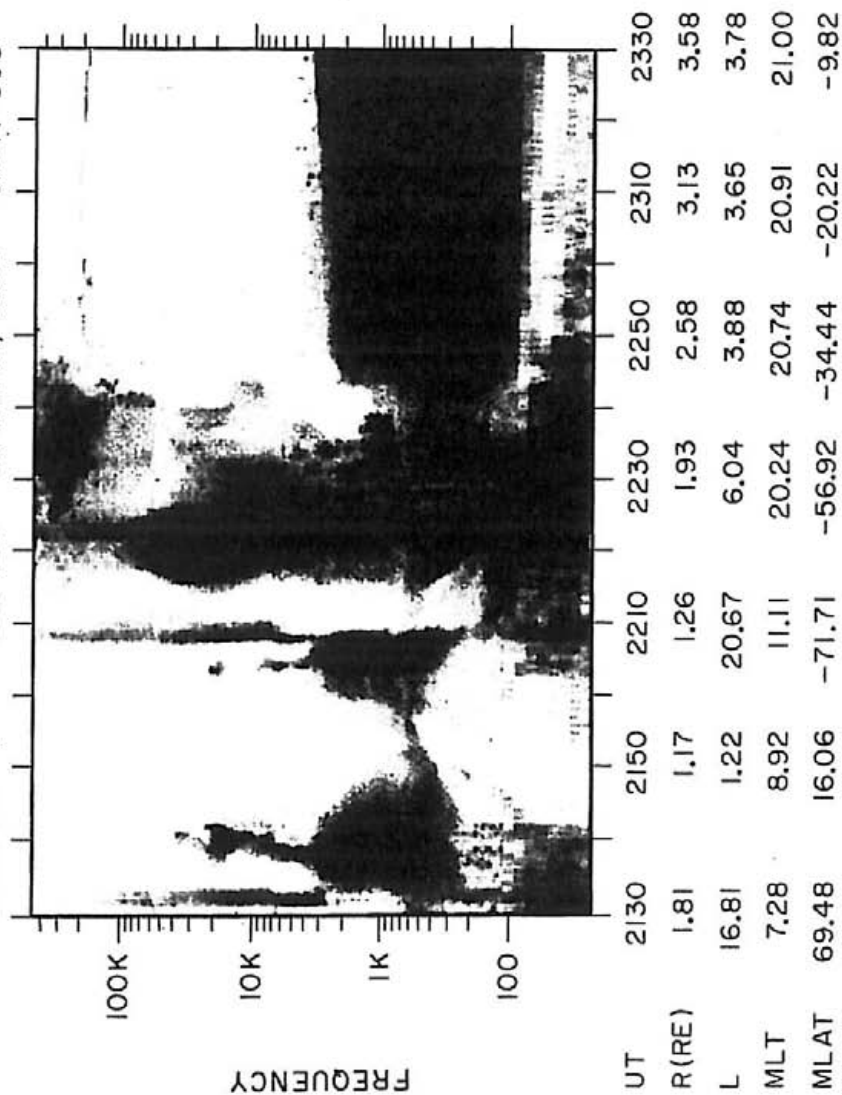


Figure 30

Figure 31 Example of an unusual, low latitude electric field found on a magnetic field line coincident with an SAR arc. This data is from day 81293 (October 20, 1981). The graph spans only 16 minutes of time. The peak in the E_{\perp} plot occurs at 14:11 UT, when DE-1 was on an L shell of 2.82, which translates to an invariant latitude of 53° . At the same time, an SAR arc was detected with ground-based photometers. The location of the arc was 53° INVLAT.

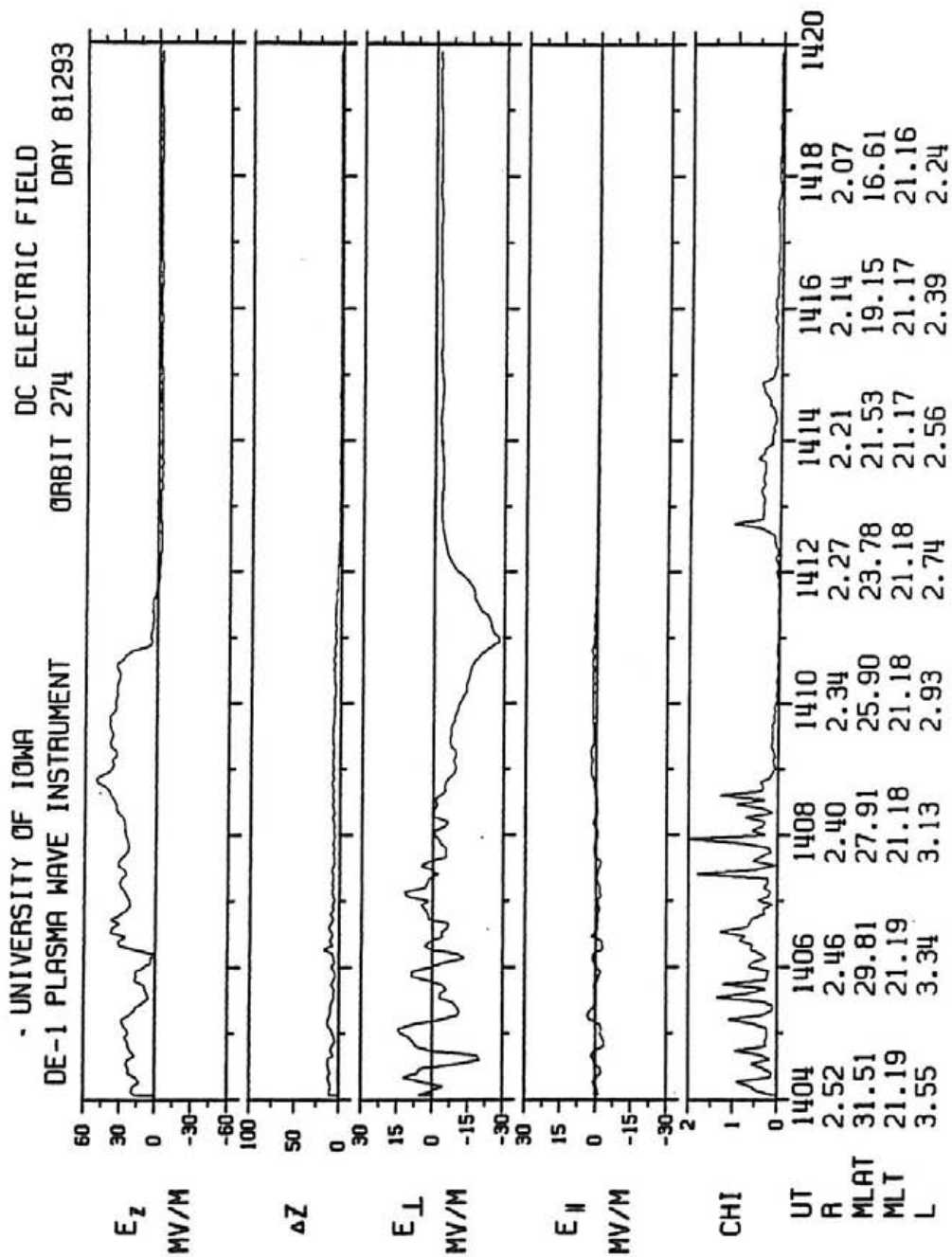


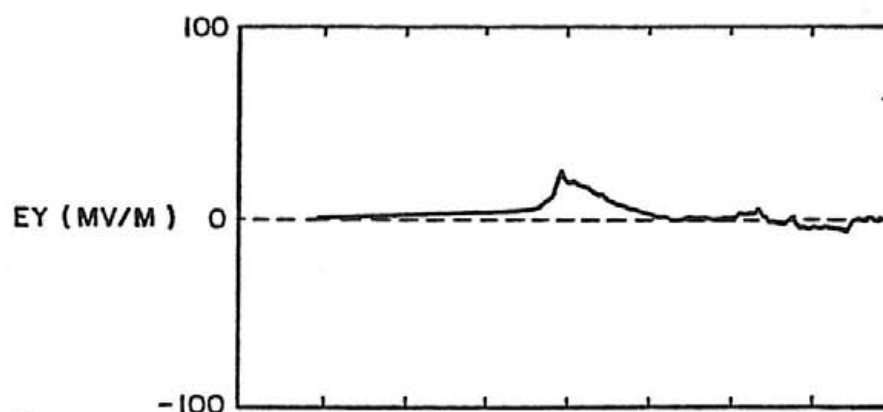
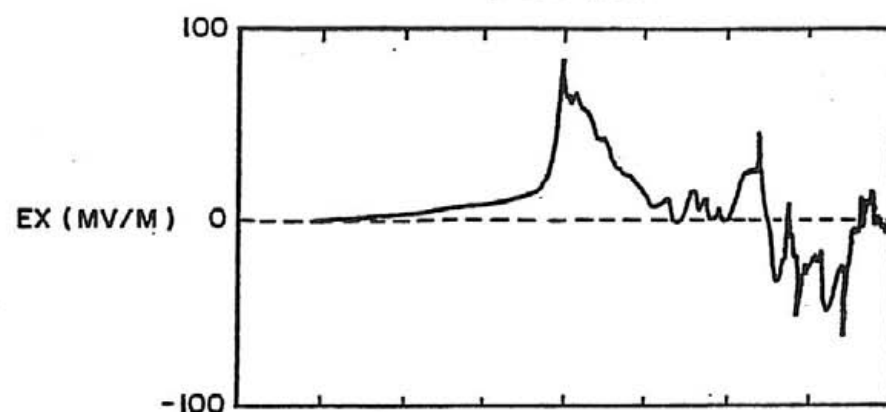
Figure 31

Figure 32

Electric field measurement from the VEFI experiment on the low-altitude DE-2 spacecraft. This data was obtained 70 minutes prior to the data shown in figure 31. DE-2 was on the same magnetic field lines but in the opposite hemisphere, so the electric field is a mirror image of the DE-1 data.

A-683-273

DE -B VEFI 20 OCT 1981 - 81293 COORD: SPC
ORBIT 1153



UT	13:16	13:18	13:20	13:22	13:24
INV. LAT.	39.9	48.2	56.5	64.6	72.6
MLT (H)	21.1	21.1	21.1	21.1	21.1
GLAT	-26.7	-34.3	-42.0	-49.7	-57.5
GLONG	112	112	111	111	110
ALT (KM)	564	527	491	458	428

Figure 32